



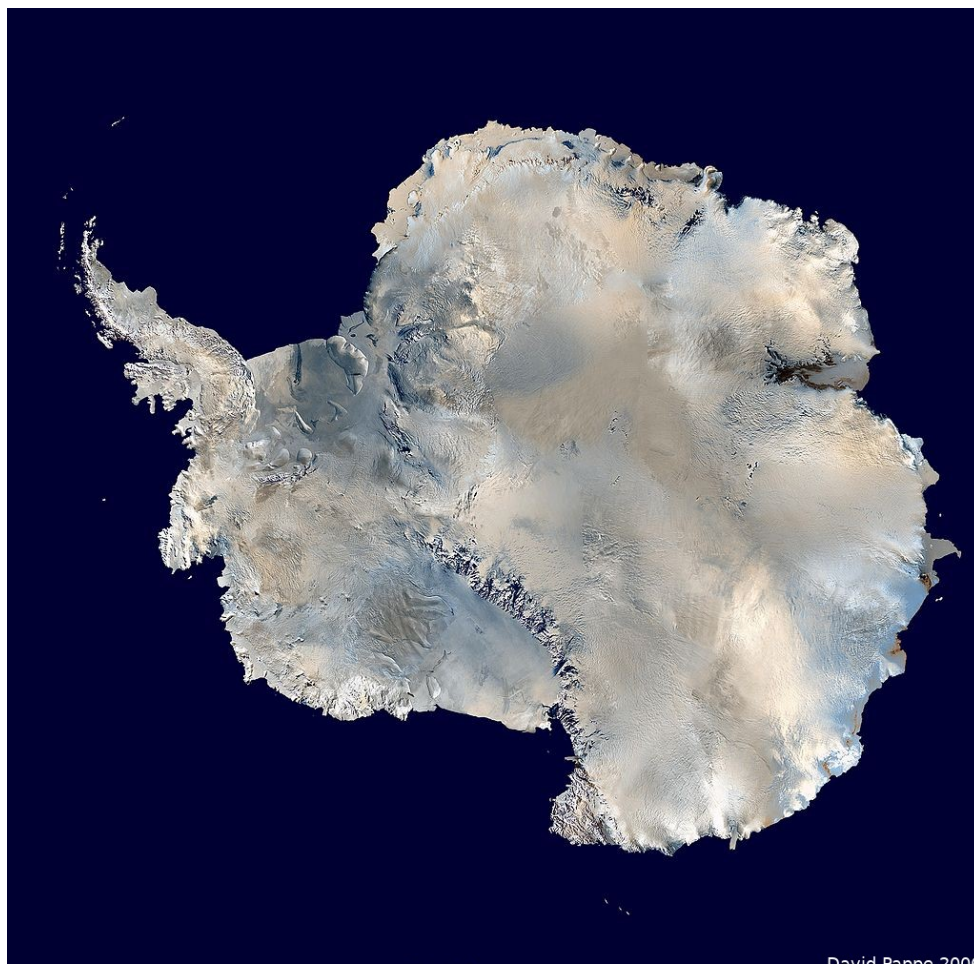
The Danish  
Meteorological  
Institute

# DMI Report 21-23 A prototype of the coupled EC-Earth-PISM model comprising the Antarctic Ice Sheet

Final scientific report of the 2020 National Centre for Climate Research Work Package 1.1.3, IskappeANT

DMI Report  
15 January 2021

By  [0000-0003-3110-3857](https://orcid.org/0000-0003-3110-3857) Christian B. Rodehacke, Marianne S. Madsen, and Paul Gierz



## Colophon

<b>Serial title</b>	DMI Report
<b>Title</b>	DMI Report 21-23 A prototype of the coupled EC-Earth-PISM model comprising the Antarctic Ice Sheet
<b>Subtitle</b>	Final scientific report of the 2020 National Centre for Climate Research Work Package 1.1.3, IskappeANT
<b>Author(s)</b>	 <a href="https://orcid.org/0000-0003-3110-3857">0000-0003-3110-3857</a> Christian B. Rodehacke, Marianne S. Madsen, and Paul Gierz
<b>Other contributors</b>	Paul Gierz, Alfred Wegener Institute for Polar and Marine Research, Bremerhaven, Germany
<b>Responsible institution</b>	Danish Meteorological Institute
<b>Language</b>	English
<b>Keywords</b>	climate modelling; EC-Earth; ice sheet modelling; Parallel Ice Sheet Model; PISM; scope-coupler; coupled climate ice sheet model; ocean-ice sheet interaction; Antarctica; Southern Ocean; sea level [Text]
<b>URL</b>	<a href="https://www.dmi.dk/publikationer/">https://www.dmi.dk/publikationer/</a>
<b>Digital ISBN</b>	978-87-7478-697-9
<b>ISSN</b>	2445-9127
<b>Version</b>	15 January 2021
<b>Website</b>	<a href="http://www.dmi.dk">www.dmi.dk</a>
<b>Copyright</b>	DMI

## Content

<b>1</b>	<b>Abstract</b> .....	<b>4</b>
<b>2</b>	<b>Resumé</b> .....	<b>4</b>
<b>3</b>	<b>Introduction</b> .....	<b>4</b>
3.1	Ice Sheets .....	5
3.2	Antarctica .....	5
3.2.1	Mass Balance of Antarctica .....	6
3.3	Ocean-Ice Shelf Interaction .....	6
3.4	Coupling between and Ice Sheet and Climate Model .....	6
<b>4</b>	<b>Models</b> .....	<b>7</b>
4.1	EC-Earth .....	7
4.2	Parallel Ice Sheet Model (PISM) .....	8
<b>5</b>	<b>Coupling Strategy</b> .....	<b>9</b>
5.1	Ice Sheet Spin-up .....	9
<b>6</b>	<b>EC-Earth's Preindustrial Climate in Comparison to Climatological Data Sets</b> .....	<b>10</b>
6.1	2m-Air Temperature .....	10
6.2	Precipitation .....	12
6.3	Surface Mass Balance via Tuning of the PDD Approach .....	12
6.4	The Ocean's Salinity .....	14
6.5	The Ocean's Potential Temperature .....	15
<b>7</b>	<b>Coupling via PICO</b> .....	<b>16</b>
<b>8</b>	<b>Discussion</b> .....	<b>17</b>
8.1	Consequences of the Climatological Biases .....	17
8.2	Examples of transformed fields from EC-Earth to PISM and vice versa .....	18
<b>9</b>	<b>Conclusion</b> .....	<b>20</b>
<b>10</b>	<b>Appendix</b> .....	<b>22</b>
<b>11</b>	<b>References</b> .....	<b>25</b>
<b>12</b>	<b>Previous reports</b> .....	<b>31</b>

## 1 Abstract

A prototype of a coupled climate-ice sheet model has been developed by the work package 1.1.3 "IskappeANT." The coupled system comprises the climate model EC-Earth and the Parallel Ice Sheet Model (PISM), representing Antarctica. Since the direct implementation of the involved processes, such as the implementation of ice shelf geometries, the ocean-ice shelf interaction, or the computation of the surface mass balance, would exceed the funding period of one year, we exploit state-of-the-art parameterizations. However, the robust system is open for enhancements in consecutive steps afterward and allows exploring scientific frontiers. The coupled system is one of the first state-of-the-art global climate models where the climate system interacts with the Antarctic ice sheet and its fringing ice shelves. This ambitious package includes these tasks: infrastructure to run the Parallel Ice Sheet Model (PISM) version 1.1.4 and version 1.2, setup and configuration of PISM to simulate Antarctica as a standalone model, coupling infrastructure, and first coupled simulations. This document describes the design decisions of the coupling. It presents the analysis of the preindustrial climate state in the Southern Ocean and across Antarctica. These states are subject to sufficiently large biases suggesting anomaly coupling between the climate model and the ice sheet model as an adequate coupling strategy.

## 2 Resumé

WP 1.1.3 "IskappeANT" har udviklet en prototype af et koblet klima-iskappe modelsystem. Det koblede system består af klimamodellen EC-Earth og iskappemodellen PISM, der repræsenterer den Antarktiske iskappe. Vi benytter os af de nyeste state-of-the-art parameteriseringer, da den direkte implementering af de involverede processer, fx ishylde-geometrier, vekselvirkningen mellem hav og ishylde eller beregningen af overflademassbalancen er for omfattende til et 1-årigt projekt. Modelsystemet vil løbende kunne udvikles og gøre det muligt at afprøve nye videnskabelige metoder. Det koblede system er blandt de første globale klimamodeller, der er fuldt koblet til en model af den Antarktiske iskappe og de omkransende ishylder. Denne ambitiøse arbejdsplan indeholder følgende opgaver:

Infrastruktur til at køre PISM version 1.1.4 og 1.2, opsætning og konfiguration af PISM for stand-alone simulering af Antarktis, infrastruktur til kobling mellem klima- og iskappemodel og de første koblede modelkørsler. Denne rapport beskriver de overordnede beslutninger i forhold til koblingsstrategien. Den præsenterer en analyse af det før-industrielle klima for Antarktis og Sydhavet. Dette klima har så store bias at det vil være mest oplagt at anvende anomalier i koblingen mellem klima- og iskappemodel.

## 3 Introduction

The Danish National Centre for Climate Research (Nationalt Center for Klimaforskning, NCKF) has completed its first year in 2020. It has been a source of funding for the Danish Meteorological Institute and collaborators for climate change related research during this year. The 18 work packages fall under four general themes:

1. Arctic and Antarctic Research
2. Climate change in the near future
3. Use of climate data
4. Support for the IPCC

The work package 1.1.3 (IskappeANT) contributes to the general themes 1, 2, and 4. With a clear focus on Antarctica (theme 1) and planned studies addressing the future of the Antarctic ice sheet (theme 2), it will contribute naturally to the ongoing ISMIP6 (Ice Sheet Model Intercomparison Project for CMIP6; <https://www.wcrp-climate.org/modelling-wgcm-mip-catalogue/cmip6-endorsed-mips-article/1049-modelling-cmip6-ismip>) activities (theme 3). This work package interacts with the work package 1.1.1. (Indlandsisen). However, Greenland and Antarctica are different and it requires tailored approaches to couple the ice sheet model with the climate model. For ice sheets, the accumulation of precipitation, commonly fallen as snow, represents mass input that drives ice sheet growth. For Greenland, the ice loss occurs predominately by the

melting of the ice surface. In contrast, ocean-driven processes control the mass loss in Antarctica. Furthermore, the term ice sheet model stands for an ice sheet model also representing ice shelves if not otherwise said.

### 3.1 Ice Sheets

Along the low elevated margins of the Greenland ice sheet, melted snow and ice runs off if it does not refreeze in the local snowpack (Langen et al., 2015; Mottram et al., 2017; Vizcaino et al., 2015). The ice mass is reduced by this runoff (Rignot et al., 2020; Sasgen et al., 2012; Shepherd et al., 2012). For continued climate warming, amplified ice loss by enhanced surface melting seems inevitable (Vizcaino et al., 2015)(Madsen 2021 -- Climate Dynamics). Thereby surface processes are central for the coupling between a climate model and an ice sheet model representing the Greenland ice sheet.

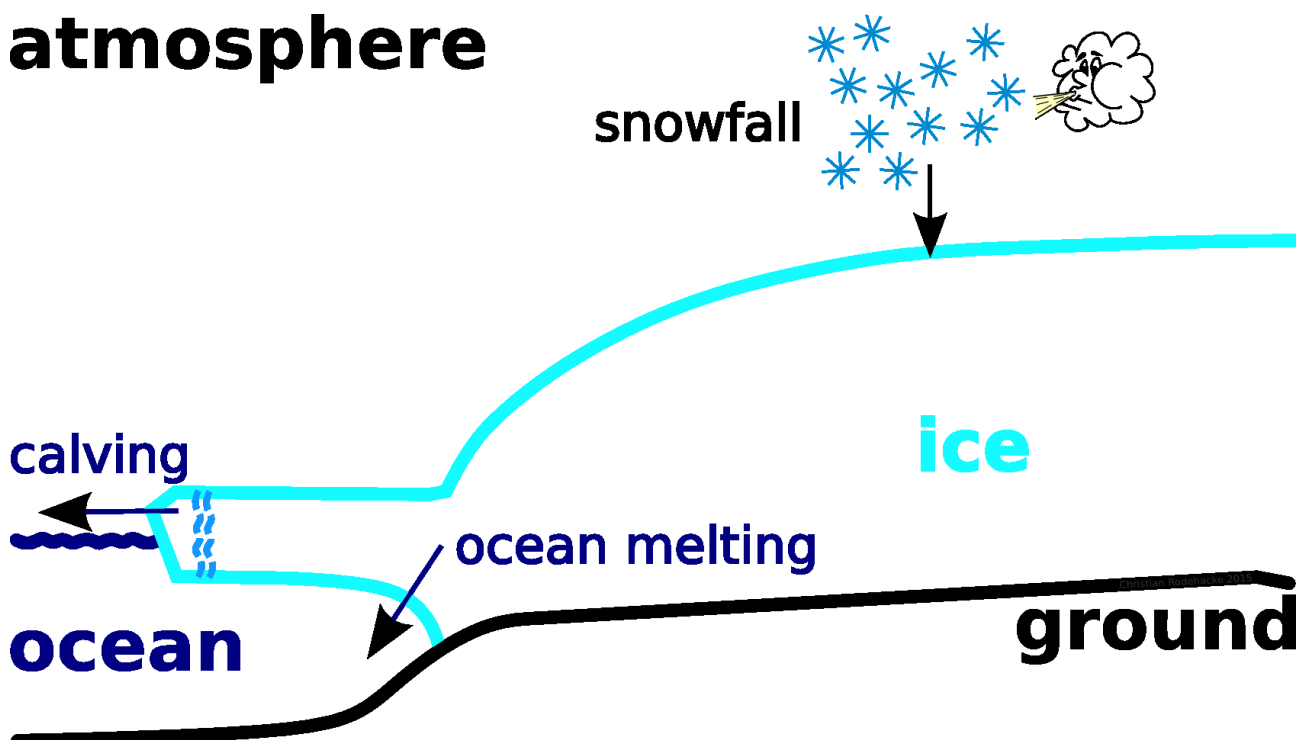


Figure 1 Sketch of the essential ice mass gain process (snowfall) and ice mass loss processes (basal melting of floating ice shelves and iceberg calving) that control the shape of Antarctica.

### 3.2 Antarctica

The region around the Southern Pole hosts the Antarctica Ice Sheet. At the pole, the ice sheet elevates 2800 m above sea level, and the plateau of the Antarctica Ice Sheet rises about 3000 m above sea level (Fretwell et al., 2013). The mean ice thickness of the West Antarctic Ice Sheet and East Antarctic Ice Sheet is 1048 m and 2146 m, respectively (Lythe and Vaughan, 2001). The Antarctic Ice Sheet, including the fringing ice shelves, has a volume of  $26.9 \cdot 10^6 \text{ km}^3$  (Fretwell et al., 2013) and covers  $13.9 \cdot 10^6 \text{ km}^2$ . The sea level potential of the West Antarctic Ice Sheet and East Antarctic Ice Sheet is 4.3 m and 53.3 m, respectively (Fretwell et al., 2013). Around Antarctica flows the Antarctic Circumpolar Current (ACC) through the Drake Passage with a baroclinic transport of 134 Sv (Cunningham, 2003);  $1 \text{ Sv} = 10^6 \text{ m}^3/\text{s}$ . The sum of the baroclinic and barotropic transport reaches 173 Sv (Donohue et al., 2016). It is the most vital circulation pattern on earth, representing 173 times the freshwater flow of all rivers globally. These settings control the climate conditions that inhibit widespread surface melting. Even though surface melting occurs along the Antarctica Peninsula (Krinner et al., 2006; Kuipers Munneke et al., 2012, 2018), this melting will grow further for ongoing climate warming (Krinner et al., 2006; Trusel et al., 2015). Also detected supraglacial surface lakes

(Stokes et al., 2019) and observed melting on ice shelves surrounding Antarctica (Bell et al., 2018) shows that runoff exists.

### 3.2.1 Mass Balance of Antarctica

In the Ross Ice Shelf sector of the Western Antarctic Ice Sheet (WAIS), atmospheric conditions related to a strong El Niño drove surface melting in 2016 (Nicolas et al., 2017). Otherwise, surface melting has been detected before across the Antarctica Ice Sheet (Liston and Winther, 2005; Schlatter, 1972; Tedesco, 2009). However, these melting events do not change the mass balance because it refreezes regionally in the snowpack (Agosta et al., 2019; Liston and Winther, 2005; Schlatter, 1972).

For Antarctica's total mass balance, the runoff producing surface melting is neglectable (Rignot et al., 2019; Shepherd et al., 2019; Wingham et al., 2018). Instead, ocean-driven basal melting of flowing ice shelves and iceberg calving are the processes driving ice mass loss. Although the relative contribution of iceberg calving versus basal melting varies between 10% and 90% for individual ice shelves (Depoorter et al., 2013), the average fraction is about 1:1 across Antarctica (Depoorter et al., 2013; Liu et al., 2015; Rignot et al., 2013).

The balance between mass gain by precipitation and the mass loss of basal ice-shelf melting and iceberg calving determines Antarctica's sea-level contribution (Figure). In recent decades, heavier precipitation across Antarctica has increased the mass inflow (Bromwich et al., 2011; Frieler et al., 2015; Medley and Thomas, 2019), while also enhanced discharge reduced ice mass loss (Rignot et al., 2013), although decadal variability is strong (Velicogna et al., 2020).

### 3.3 Ocean-Ice Shelf Interaction

Modeling ocean-ice shelf interaction is challenging because the ocean (Nakayama et al., 2014) and the ice shelves (Goldberg et al., 2019) need to be resolved at sufficiently high resolution. It is also necessary to describe adequately the process chain leading to the ocean-ice shelf interaction (Dinniman et al., 2016). Atmospheric forcing, such as easterly winds flowing along the coast of Antarctica, shapes via Ekman transport the Antarctic Slope Current (Thompson et al., 2018). Although the regional conditions differ, two distinct modes are defined. The first mode is characterized by a distinctive baroclinic structure that acts as a gate preventing the penetration of warm water masses onto the continental shelf (Darelius et al., 2016; Spence et al., 2014). The regions in front of the Filchner-Ronne Ice Shelf and Ross Ice Shelf are prominent examples. In the second mode, Ekman transport lifts warm water masses enabling the flow of warm water masses on the continental shelf (Jenkins et al., 2018; Spence et al., 2014); The Amundsen Sea is a typical example.

The competition between atmospheric and ocean processes (Smith et al., 2020), which are the boosted mass gain in East Antarctica (Harig and Simons, 2015; Medley and Thomas, 2019) and enhanced mass loss along the coast in West Antarctica and the Antarctic Peninsula (Harig and Simons, 2015), leads to a net ice loss (Velicogna et al., 2020). A recent study highlights that any simulated sea-level change depends strongly on the implemented and applied precipitation condition (Rodehacke et al., 2020). Hence, it is open if the recently simulated positive sea-level contributions are robust (Golledge et al., 2015; Mengel et al., 2015; Winkelmann et al., 2012, 2015). Nevertheless, ongoing changes in the atmosphere and ocean have driven recent ice loss by ocean processes (Shepherd et al., 2019).

Since the ocean determines ice loss, it has been proposed to block the flow of warm water towards Antarctica to mitigate Antarctica's sea-level contribution (Moore et al., 2018). Simplified simulation of the ice sheet via a flow line model supports this idea (Wolovick and Moore, 2018). However, ocean simulations resolving the ocean-ice shelf interaction highlight that such a wall redirects warm water mass to other ice shelves, where the melting is amplified (Gürses et al., 2019).

### 3.4 Coupling between and Ice Sheet and Climate Model

Since the ocean-ice shelf processes are central for Antarctica's mass balance, ocean and ice sheet/ice-shelf models have been coupled (Favier et al., 2019; Timmermann and Goeller, 2017). In these model systems, a changing ice shelf geometry and a moving grounding line affect both submodels. Hence, such models are a valuable tool to study this dynamic system. A different approach is taken by Kreuzer (Kreuzer et al., 2020) by coupling the ocean model MOM5 with the Parallel Ice Sheet Model (PISM) via the PICO model (Reese et al.,

2018). As part of PISM, the PICO model simulates the overturning circulation in shelf ice caverns. PICO is based on a box model representing the "ice pump" circulation (Olbers and Hellmer, 2010). These coupled ocean-ice sheet models do not include any atmospheric processes or any feedback between ocean and atmosphere. Thus, the ocean-ice shelf interaction does not impact the atmosphere. Hence, it is unclear how to handle a retreating ice shelf because it would make any existing climatological atmospheric forcing obsolete. Therefore, amplifying or damping effects by a changing atmosphere, which enhances or inhibits the flow of warm water masses into ice shelf caverns, are not represented.

The climate-ice sheet interaction has been implemented at various levels of sophistication. Based on coupled ocean-atmosphere simulations, Abe-Ouchi et al. (Abe-Ouchi et al., 2013) developed a climate parameterization to perform stand-alone ice-sheet simulations. The integration of ice sheet models representing Antarctica has been done in earth system models of intermediate complexity (EMIC). For instance, Golledge et al. (Golledge et al., 2019) have coupled the EMIC LoveClim with the PISM. Sadai et al. (Sadai et al., 2020) simulate the climate response in a model of higher complexity and resolution. During the climate simulations, they apply freshwater and heat flux fields obtained from pre-computed stand-alone ice-sheet simulations. These ice sheet simulations are driven by climate conditions from the same climate model under a standard setup. Besides these peer-reviewed publications, other efforts are ongoing. UKESM1 and, in particular, its ocean model NEMO, is coupled with the ice sheet model BISICLES (Siahaan and Smith, 2019). The Exascale Earth System Model (E3SM) shall be coupled with the MPAS-Albany Ice Sheet model (Asay-Davis, 2019).

In our work, we use the SCOPE (Gierz et al., 2020) to couple our climate model EC-Earth with the Parallel Ice Sheet Model (PISM). Scope implements the coupling via the exchange of forcing files between two single simulations of the climate model. Since EC-Earth does not resolve the ice shelf cavities, we exploit the PICO parameterization to implement the ocean-ice shelf coupling.

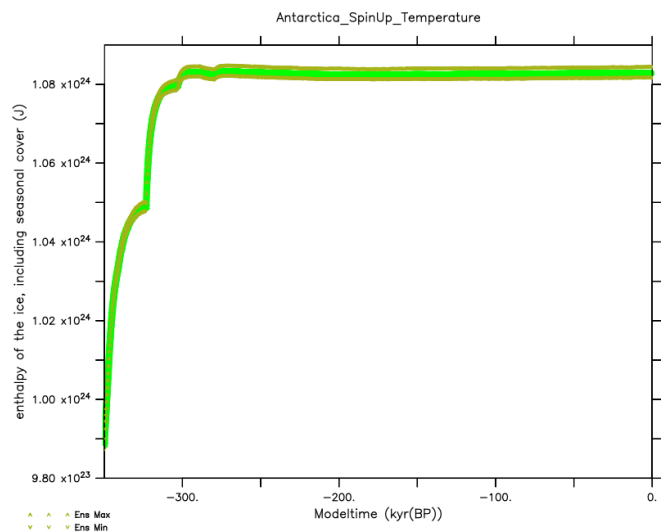


**Figure 2** The temporal evolution of the ice enthalpy cross the entire Antarctic Ice Sheet. The thick green line shows the ensemble mean value while the downward/upward-directed triangles represent the ensemble maximum and minimum, respectively. For these simulations, all mass fluxes across the outer ice boundaries are inhibited while the temperature field evolves freely.

## 4 Models

The characteristics of the climate model EC-Earth and the Parallel Ice Sheet Model (PISM) are summarized.

### 4.1 EC-Earth

The climate model EC-Earth (version 3.3) is a fully coupled atmosphere-ocean-sea ice-land model. It comprises the atmosphere model IFS (Integrated Forecasting System, cycle 36r4), the ocean model NEMO (version 3.6), the Louvain-la-Neuve sea Ice Model version 3, and the H-TESSSEL surface scheme. The coupling between the atmosphere and ocean-sea ice is established via the Ocean Atmosphere Sea Ice Soil coupler version 3 – OASIS3 (Craig et al., 2017).

The atmosphere is a primitive equation model from the European Centre for Medium-Range Weather Forecasts (ECMWF). Horizontally, it has a spectral resolution of T255, corresponding to about 80 km, and 91 levels resolve the vertical up to an air pressure of 1 hPa. The NEMO ocean uses the ORCA1 configuration with a spatial resolution of about 1° around Antarctica. In the vertical, the z-coordinate has 75 layers with a

generally downward increasing layer thickness from 1 m to 200 m. The LIM3 ice model uses five ice thickness categories.

## 4.2 Parallel Ice Sheet Model (PISM)

In this study, we use the Parallel Ice Sheet Model (PISM, version 1.2) that combines the shallow ice approximation (SIA) and shallow shelf approximation (SSA) on an equidistant grid. The basal resistance is implemented as plastic till by a Mohr-Coulomb formula to compute the yield stress (Bueler and Brown, 2009; Schoof, 2006). We apply a Positive Degree Day (PDD) formulation to determine the surface mass balance (Hock, 2003; Reeh, 1991) to allow for potential melting under extreme warming scenarios.

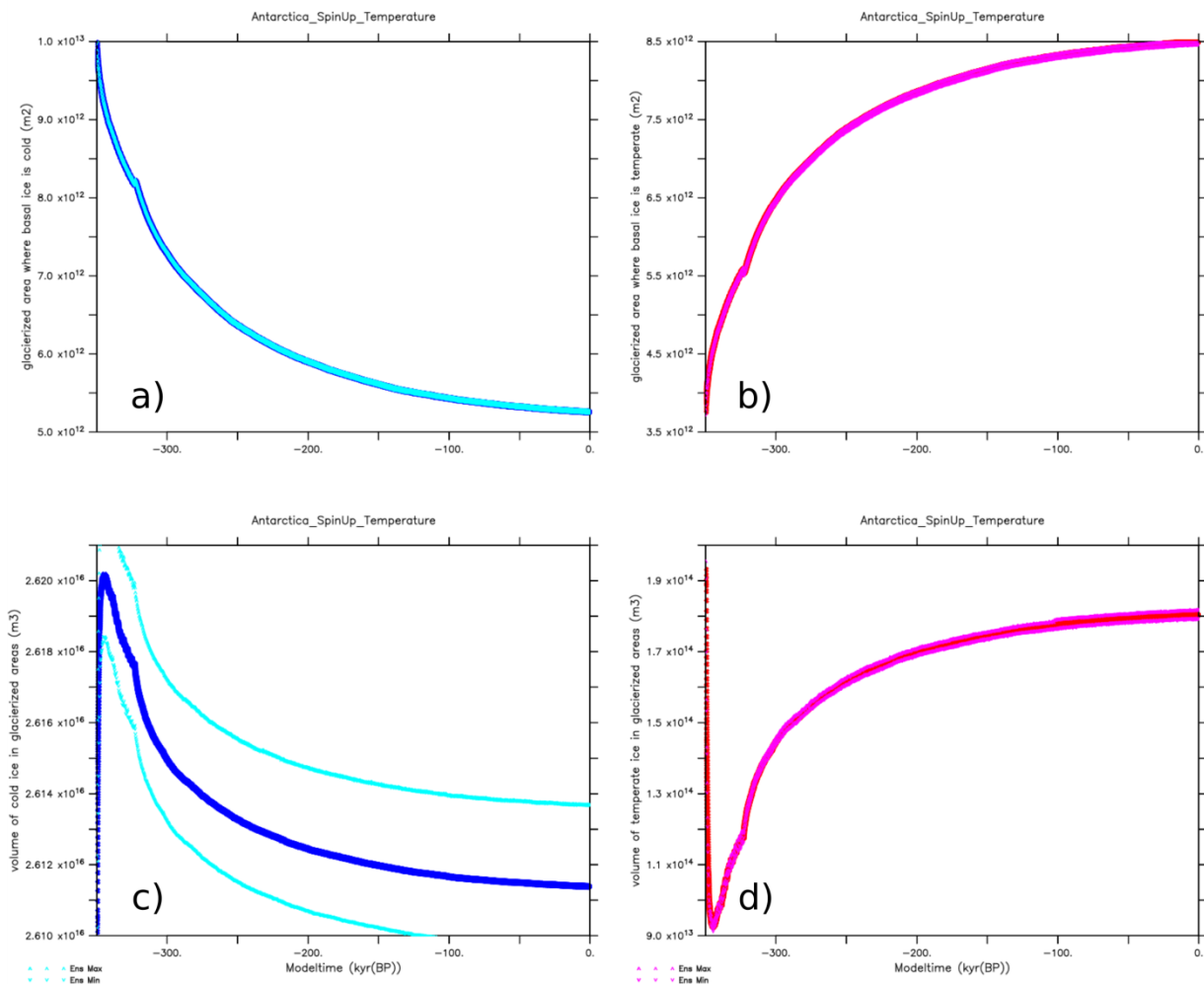


**Figure 3** As in Figure 2, the temporal evolution of the Antarctica Ice Sheet. The subfigures a) and b) depicts the development of the area covered by cold and temperate ice, respectively. The subfigures c) and d) show the related evolution of the cold and temperate ice volume, respectively.

The PICO model computes the basal melting in flowing ice shelves (Reese et al., 2018). It occurs in fully floating grid points, while the grounding line position is determined on a sub-grid space (Feldmann et al., 2014) to interpolate basal friction. We use three calving parameterizations that work at the seaward side of the ice shelf margins. First, thickness calving is enforced for shelf ice at the margin with a thickness of less than a given threshold. The thickness threshold is determined during the spinup. Ice that crosses the continental shelf edge and flows into the ocean, calves. Therefore, we have defined a calving mask that

follows approximately the contemporary 1500 m depth contour. The third parameterization exploits the Eigen-calving, which evaluates the divergent strain or velocity distribution (Levermann et al., 2012). The related proportionality constant is determined during the spinup. Former studies have shown that his proportionality constant can vary by several orders of magnitude. The viscoelastic Lingle-Clark model (Bueler et al., 2007; Lingle and Clark, 1985) acts as an isostatic submodel without the elastic part.

## 5 Coupling Strategy

The coupling strategy follows the current state-of-the-art script-based coupling between climate models and ice sheet models. For the coupling, we use the SCOPE coupler (Gierz et al., 2020). In the following, we recap the coupling scheme.

After running the climate models, atmospheric and oceanographic forcing fields are prepared and transformed onto the ice sheet grid. These climate forcing files drive the ice sheet model. Afterward, the ice sheet model output provides the freshwater flux from the basal melting of grounded ice. The output files also offer the freshwater fluxes of floating ice due to basal ice-shelf melting and iceberg calving. These are combined into one flux, and the associated heat to melt the related ice is calculated. Changes of the ice sheet geometry related to ice dynamic and the isostatic rebound compute internally in PISM give the updated surface elevation. A modification of ice extent produces an updated ice sheet mask. All these fields are transformed on the grids of the receiving climate model components. It is currently work in progress that these fields are read and taken into account during the restart and the next climate model simulation chunk. This next climate simulation starts the next loop in the coupling cycle. Before this coupling can be achieved, the Parallel Ice Sheet Model (PISM) has been spun-up.

### 5.1 Ice Sheet Spin-up

As part of the preparation before coupling EC-Earth and PISM, we have to spin up the ice sheet independently to reduce the drift once these two models are combined. Therefore, we start PISM from the currently observed geometry and run an initial simulation for a few hundred years. Afterward, we keep the geometry fixed by suppressing any mass flux through the outer ice interfaces (PISM flag `-no_mass`). We have to apply our climatological atmospheric forcing for about 350 000 years before achieving a thermal distribution in a quasi-equilibrium state.

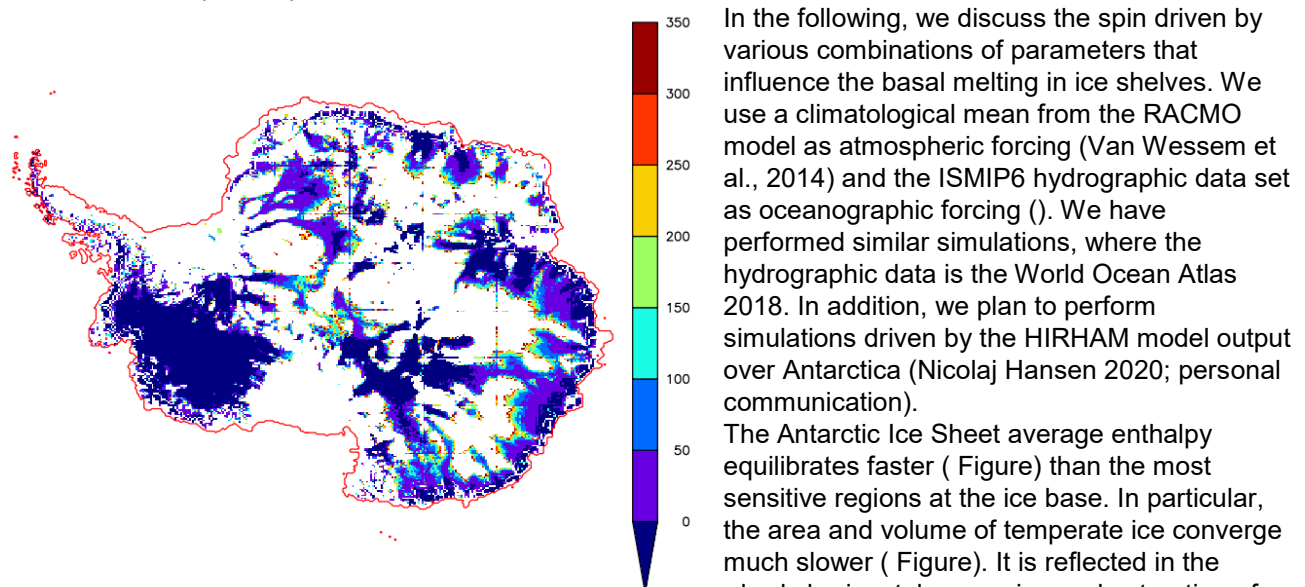
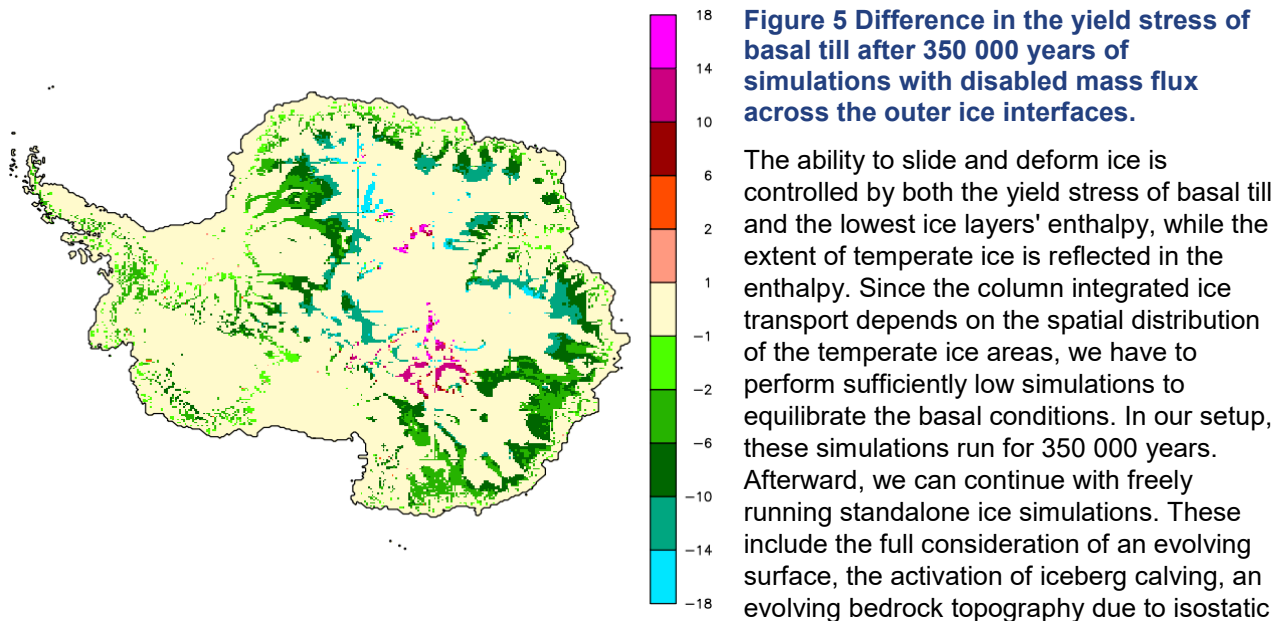


**Figure 4** The spatial map depicts the occurrence of subglacial water in basal till. The timing is relative to the simulation's start with disabled mass flux across the outer ice interfaces.

The Antarctic Ice Sheet average enthalpy equilibrates faster ( Figure) than the most sensitive regions at the ice base. In particular, the area and volume of temperate ice converge much slower ( Figure). It is reflected in the slowly horizontal expansion and saturation of subglacial water stored in the till ( Figure). As a consequence, the related yield stress of the basal till develops gradually too. In general, this yield stress decreases for areas where

subglacial water has started to saturate the basal till. However, few places in central East Antarctica are subject to a distinct increase in yield stress ( Figure).



processes, for instance.

To test the coupling, we utilize one member of the entire ensemble. As part of the developed coupling infrastructure, we integrated the feature to allow anomaly coupling from the climate model to the ice sheet model.

Here, we follow the so-called equilibrium spinup approach, where we apply a climatological forcing until the ice sheet has reached its quasi-equilibrium while the final ice sheet shall match the currently observed state. Our target is an Antarctic Ice Sheet that comprises the major ice shelves, namely the Ross Ice Shelf in the Pacific sector and the Filchner-Ronne Ice Shelf in the Atlantic sector, and the overall ice sheet geometry shall resemble the current state.

## 6 EC-Earth's Preindustrial Climate in Comparison to Climatological Data Sets

Once we combine the ice sheet model with the climate model, we have to bring this coupled system into its quasi-equilibrium. Therefore, the input flux that drives the growth shall be balanced by the ice loss fluxes on average. To estimate if this is feasible with the climate delivered by the climate model, we compare EC-Earth's preindustrial climate with contemporary climatological estimates. Although the preindustrial climate is colder than the present state, we compare the steady-state of the control simulations under the preindustrial climate with climatological data sets. We use the preindustrial steady-state because a historical climate simulation does not necessarily represent the observed climate due to internal climate variability. The comparison should be viable as long as the climatology is based on the few last decades as the temperature record at the Amundsen–Scott Base at the South Pole indicates (Clem et al., 2020).

### 6.1 2m-Air Temperature

Figure shows the long-term mean 2m-air temperature. Across the entire Antarctic Ice Sheet, the reference values are  $-34.8^{\circ}\text{C}$  or  $-34.6^{\circ}\text{C}$  based on simulations with the RACMO model (Van Wessem et al., 2014) or preliminary results of the HIRHAM model (Nicolaj Hansen 2020; personal communication). If we average the temperature only over grounded ice, the corresponding average temperatures are  $-36.2^{\circ}\text{C}$  and  $-36.1^{\circ}\text{C}$ , respectively. Over the Ross Ice Shelf and Filchner-Ronne Ice Shelf, the mean temperature is not warmer

than  $-20^{\circ}\text{C}$ . The area with an average temperature colder than  $-50^{\circ}\text{C}$  covers a large part of the Antarctica plateau as part of the East Antarctic Ice Sheet. Along the coast, the temperatures are colder than  $-10^{\circ}\text{C}$ . Temperatures above  $-10^{\circ}\text{C}$  appear at the northern Antarctica Peninsula.

The temperature distribution of the preindustrial climate has a similar structure. The Antarctic plateau is the coldest region, a ring of warmer temperatures extend along the coast, and the highest temperatures occur at the northern tip of the Antarctic Peninsula. However, across the entire continent, the temperature is  $5.9^{\circ}\text{C}$  or  $5.7^{\circ}\text{C}$  warmer than RACMO or HIRHAM, respectively. The detailed temperature difference distribution highlights some small scale fluctuations driven by topographic hummocks that are not resolved by the global climate model.

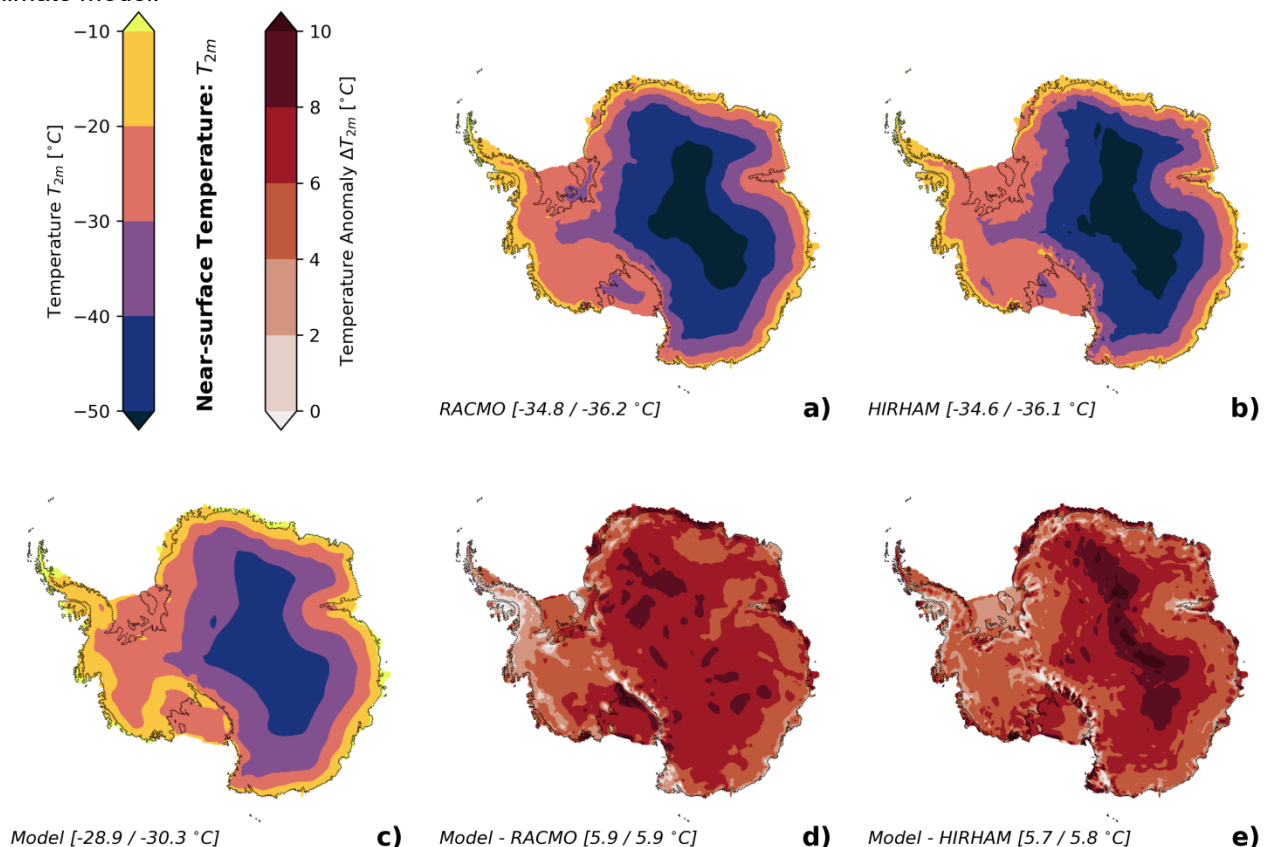


**Figure 6** 2m-air temperature over Antarctica. The subplots a) and b) show the average 2m-air temperature of the regional climate models RACMO (a) and HIRHAM (b), respectively. ERA-Interim has forced them. The lower left subplot c) depicts the temperature of preindustrial simulations with EC-Earth. These subplots use the left colorbar. The subplots d) and e) are the temperature difference between EC-Earth and RACMO, and EC-Earth and HIRHAM. These different plots use the right colorbar. Below each subfigure, the numbers in the square brackets report the average. The first number is the value across the entire plot covering Antarctica, while the second number's value is restricted to grounded ice. The black dashed line represents the grounding line position that encloses grounded ice.

Of particular interest are the high temperature anomalies over the Ross Ice Shelf north of the Antarctic Mountains (Figured, e). It is partly related to the c-shaped warm structure with a temperature above  $-20^{\circ}\text{C}$  over the West Antarctic Ice Sheet and Ross Ice Shelf (Figurec). These anomalies can punctuate a too thin Ross Ice Shelf and trigger afterward iceberg calving that weakens the Ross Ice Shelf. Such an event might be at work between second 2 and second 6 in the supplementary material of Garbe et al. (Garbe et al., 2020) Supplementary Video 1 at [https://static-content.springer.com/esm/art%3A10.1038%2Fs41586-020-2727-5/MediaObjects/41586\\_2020\\_2727\\_MOESM1\\_ESM.mp4](https://static-content.springer.com/esm/art%3A10.1038%2Fs41586-020-2727-5/MediaObjects/41586_2020_2727_MOESM1_ESM.mp4).

## 6.2 Precipitation

The total precipitation across the Antarctic (Figure) delivers in total 2550 Gt/year or 2910 Gt/year according to RACMO (Van Wessem et al., 2014) or HIRHAM (Nicolaj Hansen 2020; personal communication). If we restrict the accumulation area to grounded ice, the reported yearly mass gain is 2080 Gt/year or 2370 Gt/year, respectively. These simulations highlight that the Antarctic interior is a desert because it receives less than 100 mm precipitation per year. More precipitation falls along the coasts, where a rising surface triggers topographic precipitation when incoming storms are lifted upward on their way inward. The wettest region is the coastal strip of the West Antarctic Ice Sheet that extends eastward from the Ross Ice Shelf via the Amundsen Sea up to the northern tip of the Antarctic Peninsula.

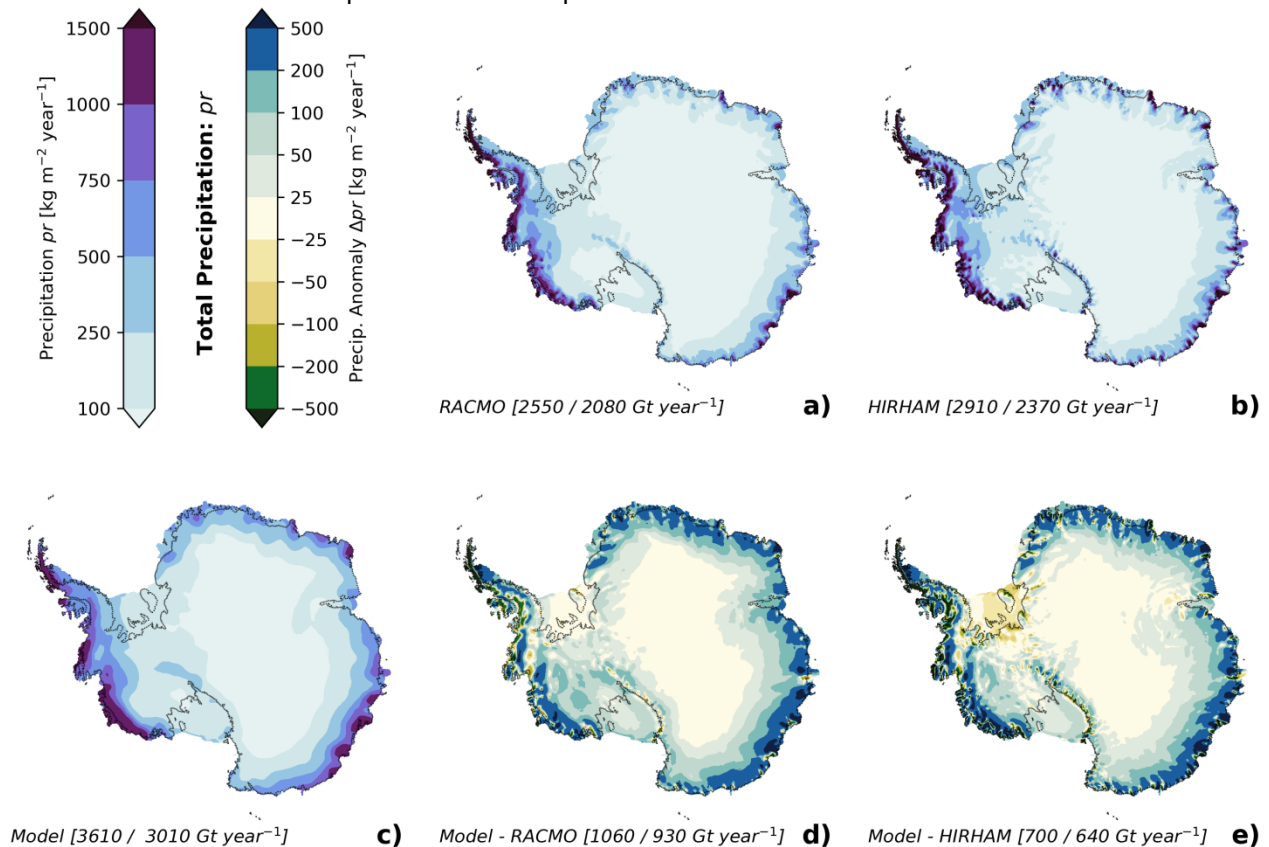


**Figure 7** Like Figure 6, but it depicts precipitation over Antarctica. The subplots a) and b) show the average precipitation of RACMO (a) and HIRHAM (b), respectively. The lower left subplot c) depicts precipitation of EC-Earth. The subplots d) and e) are the precipitation difference between EC-Earth and RACMO, and EC-Earth and HIRHAM. Below each subfigure, the squared brackets report the integrated amount. The first number is the value across the whole of Antarctica, while the second number's value is restricted to grounded ice. The black dashed line follows the grounding line.

EC-Earth simulates a desert across the Antarctic plateau and more precipitation along the coasts. The integrated precipitation across the continent or the ground ice area amounts to 3610 Gt/year or 3010 Gt/year. Hence, EC-Earth's precipitation fallen on Antarctica exceeds the estimates by 1060 Gt/year and 700 Gt/year, respectively. These differences correspond to 41% and 24% of RACMO's and HIRHAM's values, respectively. The overall wetter coasts probably drive these large differences, as the difference plots reveal (Figure 7, e).

## 6.3 Surface Mass Balance via Tuning of the PDD Approach

Supposed tuning the Degree Day Factors (DDF) of the Positive Degree Day approach, beyond common values, would correctly compute the surface mass balance. We analyze how large the DDFs would have to be and if they would exceed common DDF values for snow in the range of 3 mm/day/°C to 12 mm/day/°C,

and large values for ice commonly between 5 mm/day/°C and 20 mm/day/°C (Hock, 2003). A DDF represents the susceptibility of a snow or ice surface to conditions driving surface melting, such as shading that lowers melting or enhanced melting due to a darkened surface by added impurities. Shading leads to a lower DDF, while a darkening calls for a higher DDF. For the Khumbu Glacier in Nepal, the debris-free glacier requires a DDF (16.9 mm/day/°C); it is a common value. However, a thin debris layer of 0.3 cm and 2 cm results in a large DDF factor of 37.2 mm/day/°C and 26.0 mm/day/°C, respectively (Kayastha et al., 2000). In contrast, an even thicker layer protects the ice from radiation and turbulent heat flux, which explains that a 40cm thicker debris layer requires a small value of 5.3 mm/day/°C (Kayastha et al., 2000). Although it seems reasonable to assume that DDF factors are limited, we consider the DDF factors as freely adjustable parameters. While exploring the range of DDFs, we also investigate if EC-Earth's 2m-air temperature or the precipitation may inhibit a direct coupling.

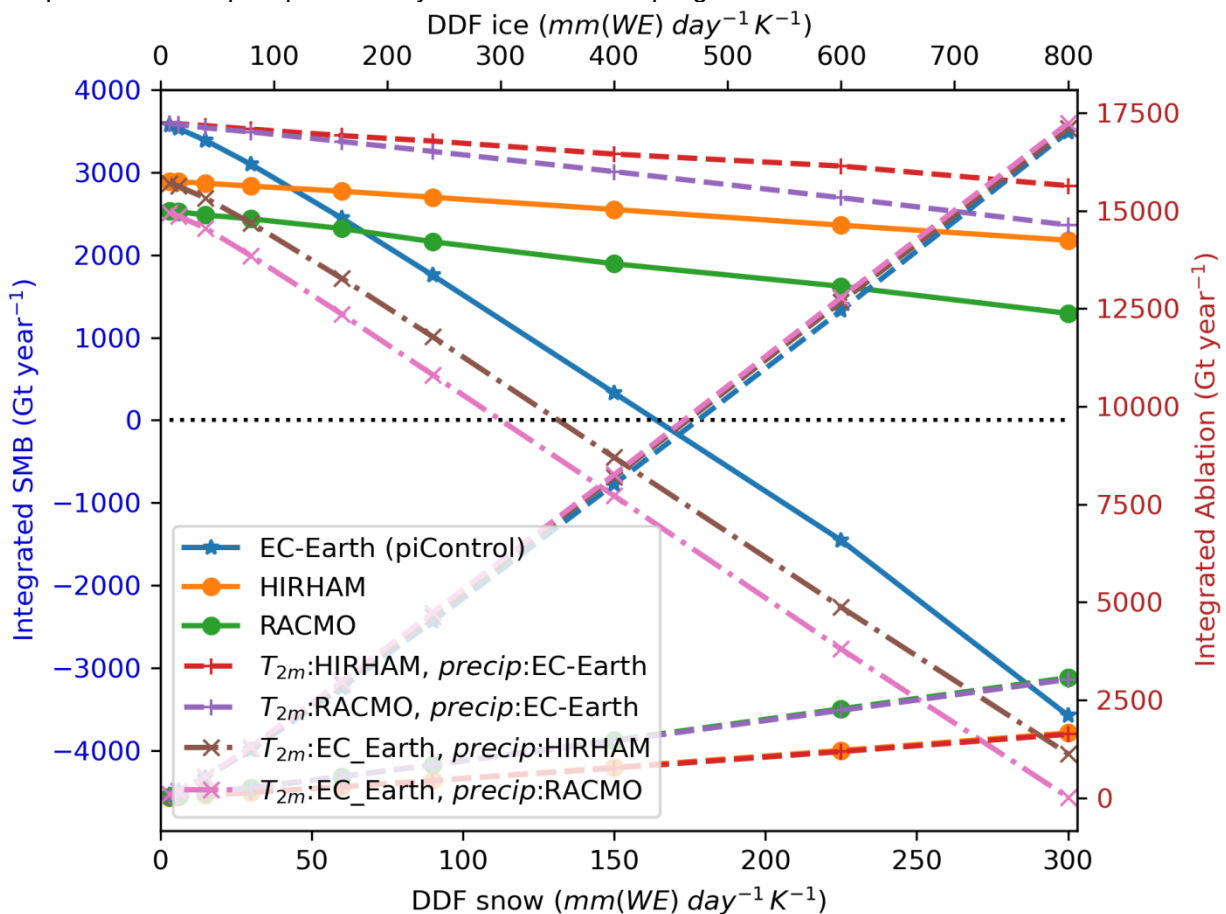


**Figure 8** The plots show two families of curves. The rightward declining curves depict the integrated surface mass balance (left y-axis with blue labels), whereas the upward rising curves represent the integrated ablation (a right x-axis with red labels). The legend shows the mean of the lines. The horizontal dotted line follows the zero surface mass balance value, at which ice loss and ice gain are balanced. The results of the first three lines labeled "EC-Earth (piControl)", "HIRHAM", and "RACMO" are obtained by using both the 2m-air temperature ( $T_{2m}$ ) and precipitation (precip) exclusively from the labeled model. The remaining curves show the results of where the temperature and precipitation come from models. The model names behind the  $T_{2m}$  and precip label indicate the used model.

For simplicity, we have here simultaneously increased the DDF for snow and ice. Figure shows the integrated surface mass balance (SMB) across Antarctica for different combinations of DDF values for snow (lower x-axis) and ice (upper x-axis). Hence, the plot contains two families of curves. This plot shows the SMB and ablation for simulations driven by temperature and precipitation from RACMO, HIRHAM, and EC-Earth. Because EC-Earth has the highest integrated precipitation (Figure), its SMB starts at the highest end,

followed by HIRHAM and RACMO. As expected, a higher pair of DDF reduces the surface mass balance (SMB) caused by amplified ablation. The temperature controls the curves' slope. Since EC-Earth has the warmest distribution (Figure), all simulations considering EC-Earth's 2m-air temperature show a distinct decrease in the SMB with increasing DDFs. Figure shows the spatial distribution of SMB and ablation for the DDF values for snow and ice of 150 mm/day/°C and 400 mm/day/°C, respectively. For this combination, the SMB is slightly positive under EC-Earth forcing. This SMB distribution would represent an Antarctic Ice Sheet that behaves like Greenland, where ablation is essential, and where low laying marginal parts of the ice sheet experience mass loss.

EC-Earth:piCtrl

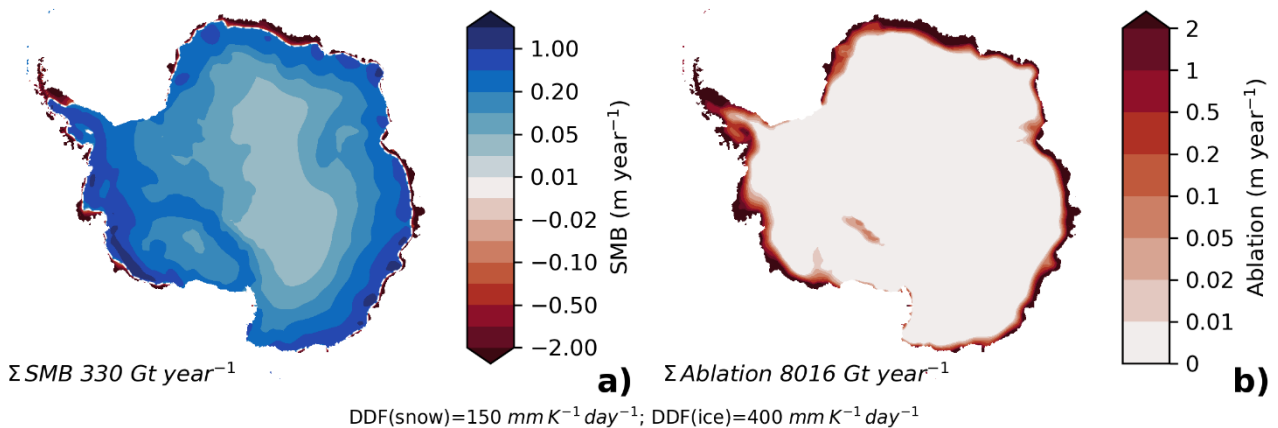


**Figure 9** The surface mass balance **a)** and ablation **b)** for simulations with EC-Earth preindustrial forcing for DDF of 150 mm/day/°C and 400 mm/day/°C. The dashed white line in the surface mass balance plot represents the equilibrium line, where mass gain and mass loss are balanced.

The high temperatures in EC-Earth allow generating a negative surface mass balance for DDF values in the middle of the scanned DDF range. Above these values, Antarctica would also lose mass at the surface. However, the required DDF values for snow above 100 mm/day/°C and ice above 250 mm/day/°C are far too high. An SMB, which is computed by EC-Earth forcing and shall be as large as the estimates from RACMO and HIRHAM, would require DDF values for snow and ice of about 40–60 mm/day/°C and 100–150 mm/day/°C. Also these values are too huge for being realistic.

## 6.4 The Ocean's Salinity

In the standard setup of EC-Earth, all precipitation fallen on Antarctica is redirected into the neighboring ocean. This procedure closes the hydrological budget under the assumption of an ice sheet in steady-state. Since the ocean's conditions control the ice loss, we inspect the upper ocean salinity and temperature distribution around Antarctica. Please note that the analyzed fields might be similar at the beginning of coupled simulations because we aim initially for a steady-state ice sheet too.

The salinity in the ocean's upper 200 m (Figure) is broadly similar in the two reference data sets: World Ocean Atlas 2018 (WOA18) and ISMIP6 (Jourdain et al., 2020). A local minimum characterizes the Weddell Gyre. A half-ring of reduced salinities extend eastward of the Weddell Gyre up to the Ross Sea as part of the Indian Ocean. A "wind vane" of lower salinities seems to develop from the Antarctic Peninsula's northern tip that progresses westward into the Pacific. The lowest salinities occur at the western edge of the Ross Ice Shelf margin near Ross Island. However, we detect differences on smaller scales that are apparently not resolved by WOA18. But these differences are small compared to the anomaly between EC-Earth and these two data sets, as we will see below. Therefore, we do not discuss these differences further.

EC-Earth reproduce the large-scale structure of higher and lower salinities connected with the large scale circulation (Figurec). However, the difference plots of EC-Earth with WOA18 (Figured) or ISMIP6 (Figuree), respectively, reveal substantial differences. Since we want to couple our ice sheet model and its ice shelves with the ocean, we restrict ourselves to differences in the coast area. In the Pacific sector between the Antarctic Peninsula and the Ross Ice Shelf, EC-Earth is saltier by up to 0.65 g/kg compared to the

references -- Please note, we report here the salinity as g/kg based on the former definition of the Practical Salinity Unit. Following the Antarctica Coastal Current that flows from the Ross Ice Shelf anticlockwise through the Indian Ocean into the Atlantic up to the Antarctic Peninsula, we detect a significantly too fresh surface ocean in EC-Earth along the entire coastal area. The salt deficit is up to 0.55 g/kg. Since salinity determines the ocean state in this cold region, a too fresh surface ocean represents an enforced lid suppressing convection.

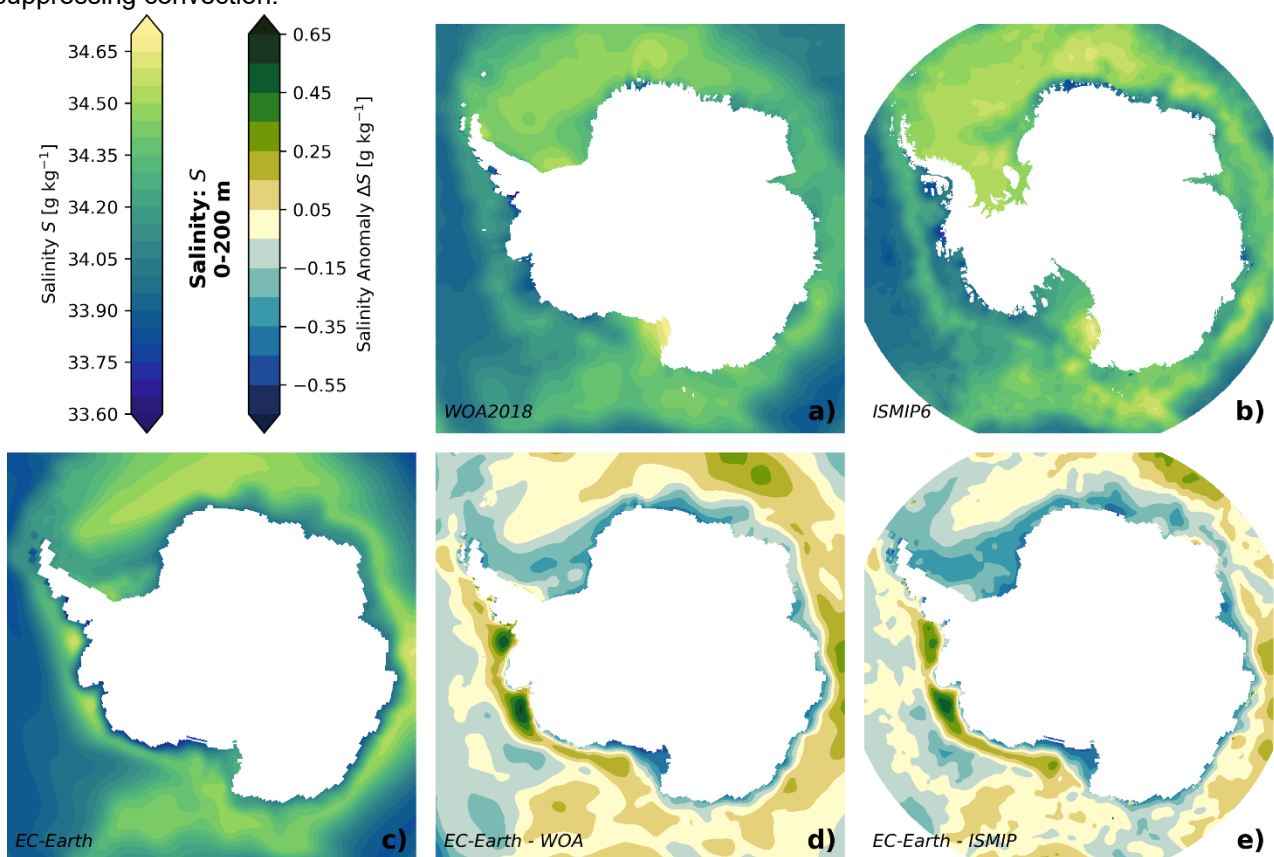


**Figure 10** Average salinity in the ocean between the surface and 200 m depth. The subplots a) and b) show the climatological mean of the World Ocean Atlas 2018 (WOA2018, WOA18) (a) and ISMIP6 prepared data set (Jourdain et al., 2020)(b), respectively. The lower left subplot c) depicts the salinity of preindustrial simulations with EC-Earth. These subplots use the left colorbar. The subplots d) and e) are the salinity difference between EC-Earth and WOA2018, and EC-Earth and ISMIP6. These different plots use the right colorbar. The white landmask is deduced from the shown data set except for ISMIP6. There we apply a mask of grounded ice derived from the BEDMAP topography data set (Fretwell et al., 2013).

## 6.5 The Ocean's Potential Temperature

Around Antarctica, the ocean potential temperature in the upper 200 m is coldest towards the coasts (Figure a, b). An extended area of coldest temperatures occurs in front of the Filchner-Ronne Ice Shelf that extends northward until the Antarctic Peninsula tip. Warm temperatures exist in the eastward flowing Antarctic Circumpolar Current (Gille2016), which appear in Figure a as warm (yellow) areas. EC-Earth reproduces this general pattern (Figure c), but overall the ocean temperatures are generally too warm (Figure d, e) except for a region around the Greenwich Meridian and in front of the Filchner-Ronne Ice Shelf. The temperature difference surpasses 2.5°C along the West Antarctic Ice Sheet coast, where we have the most vulnerable ice shelves (Khazendar et al., 2016; Milillo et al., 2019; Morlighem et al., 2020; Rignot et al., 2013, 2014; Webber et al., 2017). Such a pronounced temperature bias could prevent us from coupling EC-Earth and PISM directly because the related intense temperature forcing would melt the fringing ice

shelves that support the West Antarctic Ice Sheet. Consequently, the Marine Ice Sheet Instability (Mercer, 1978; Pattyn, 2018; Weertman, 1974) would trigger a runaway loss of the West Antarctic Ice Sheet. The average ocean temperature of the upper 800 m highlights that EC-Earth has an ocean temperature bias in front of the West Antarctic Ice Sheet. This bias is strongly pronounced in the Amundsen Sea and the Ross Sea in front of the Ross Ice Shelf.

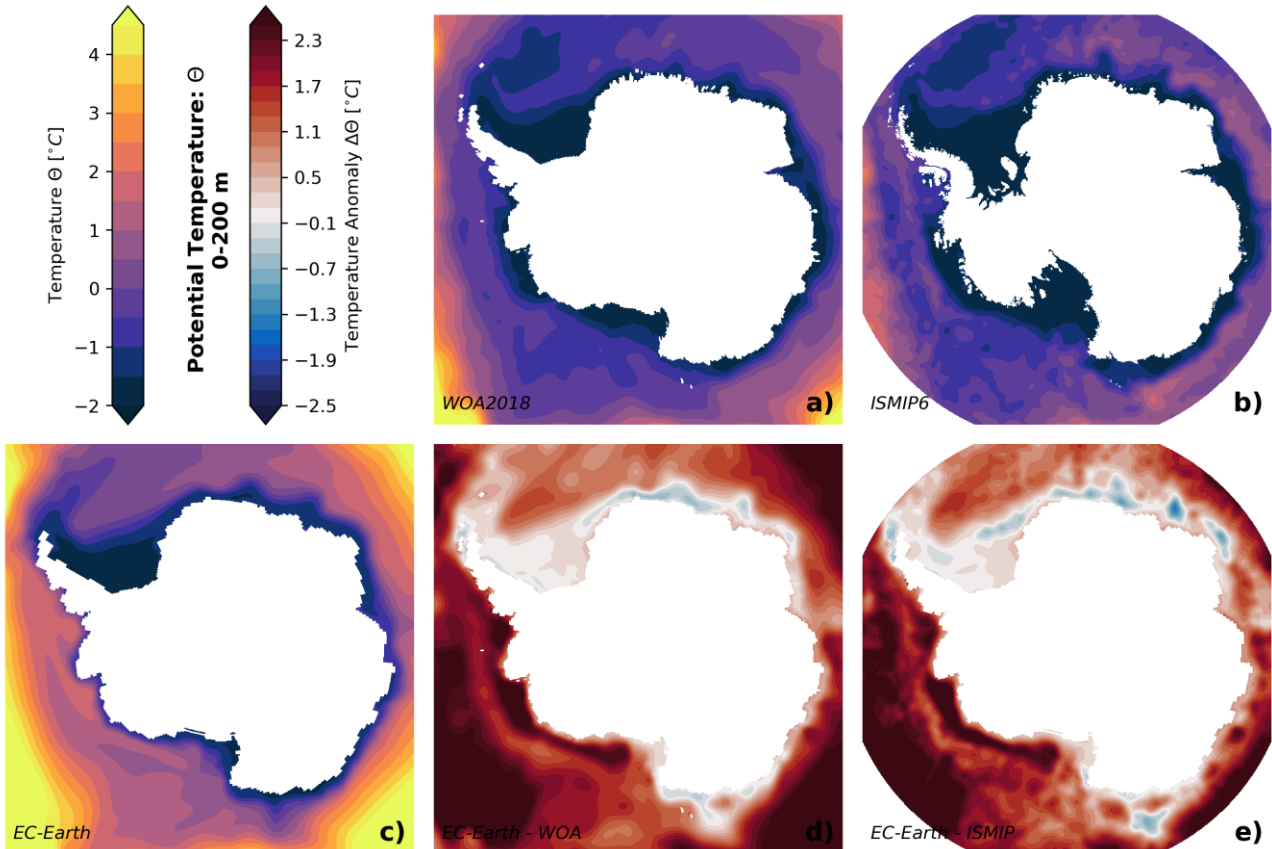


**Figure 11** Like figure 10, but displays the average potential ocean temperature between the surface and 200 m depth. The subplots a) and b) show the climatological mean of the World Ocean Atlas 2018 (WOA2018, WOA18) (a) and ISMIP6 (Jourdain et al., 2020)(b), respectively. The lower left subplot c) depicts the salinity of the EC-Earth simulation. The subplots d) and e) are the temperature difference between EC-Earth and WOA2018, and EC-Earth and ISMIP6. The white landmask stems from the shown data set except for ISMIP6, where it shows the mask of grounded ice (Fretwell et al., 2013).

## 7 Coupling via PICO

Supposed we couple initially EC-Earth with PISM, we would start from a state of a quasi-equilibrium. Under the assumption that we would have an ice sheet resembling the observed state, we try to find the combination of parameters controlling the basal melting in shelves that lead to a mass loss that corresponds to observational estimates. Therefore, we alter the parameters called "turbulent exchange velocity for temperature" and "overturning strength", while considering the two additional constraints of the PICO model (Reese et al., 2018). These require that we have basal melting at the grounding line and that the melting is smaller in the next row of grid boxes.

We use the BEDMAP ice sheet geometry (Fretwell et al., 2013) and force the model with two forcing data sets for analyzing the impact of the two PICO parameters on the total basal melt loss. First, we use the EC-Earth forcing directly, while the ISMIP6 data set (Jourdain et al., 2020) has been used as the second data set. We compare these integrated basal melting amounts with three independent estimates; Depoorter et

al. (Depoorter et al., 2013) reported a basal melting of  $(1454 \pm 174 \text{ Gt/yr})$  for the period between 1995 and 2009; Rignot et al. (Rignot et al., 2013) published a value of  $1325 \pm 235 \text{ Gt/yr}$  for the period 2003—2008; and Liu et al. (Liu et al., 2015) reported  $1516 \pm 106 \text{ Gt/yr}$  between 2005 and 2011.

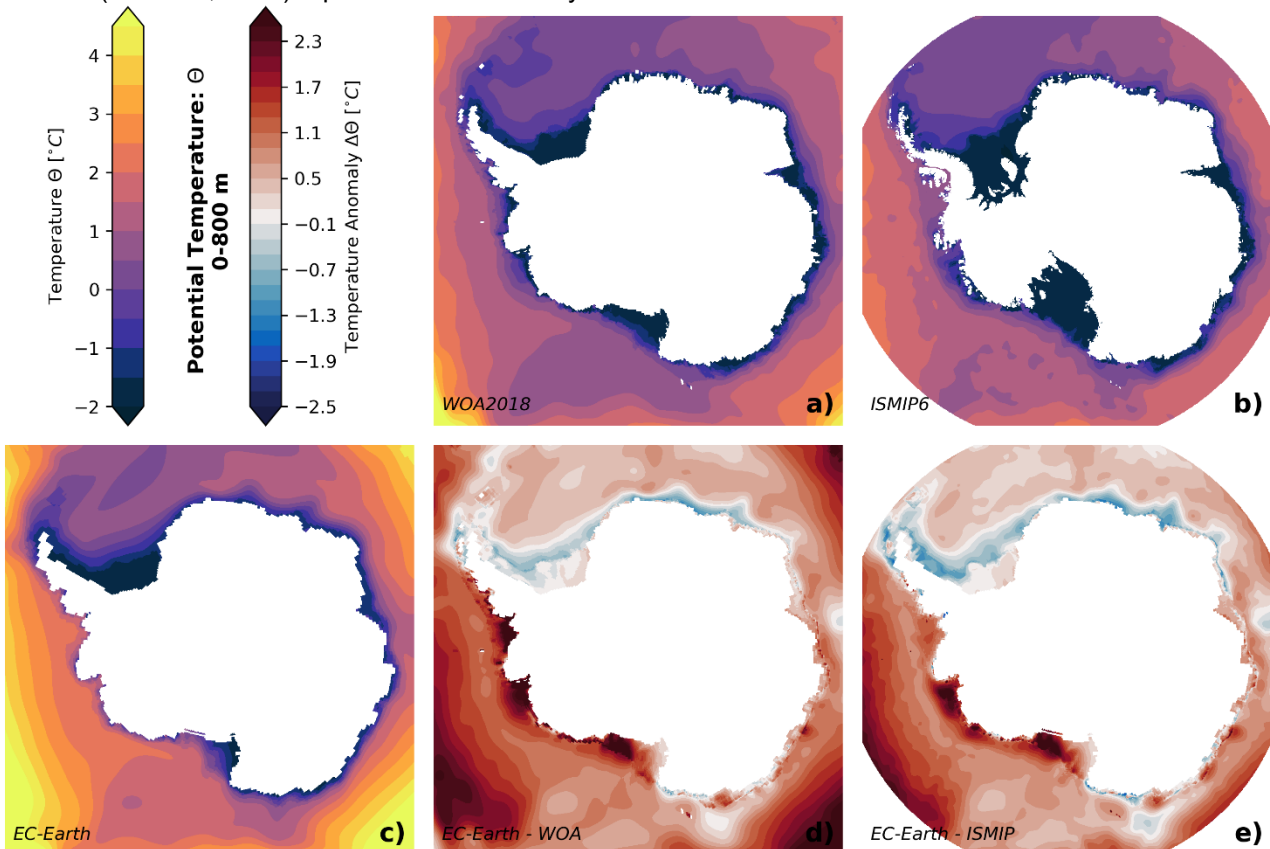


**Figure 12** Like figure 11, it displays the average potential ocean, but it expands the depth range from the surface to 800 m depth.

Supposed the ice shelves would not disintegrate under the strong thermal forcing applied along the coast of the West Antarctic Ice Sheet (Figure c), for common combinations of both parameters, we would strongly overestimate the total ice loss by basal melting. Preliminary results of an extended search reveal values that are consistent with observational estimates (not shown).

If we replace the EC-Earth forcing with ISMIP6 forcing, we find combinations of both PICO parameters that reproduce the observed basal melting. These parameter combinations are also closer to the reference value of the PICO publication (Reese et al., 2018). Here, we also have extended the search to find further combinations parameters representing the observed state (not shown).

## 8 Discussion

### 8.1 Consequences of the Climatological Biases

The atmospheric temperature bias over the Southern Ocean supports the detected excessive precipitation over Antarctica. Considering that the Antarctic Ice Sheet is in a steady-state, the amount of precipitation falling on Antarctica is released as freshwater into the ambient ocean. Since we detect along the East Antarctic Ice Sheet's coasts too intensive precipitation (Figure), the related coastal freshwater release dilutes the ocean. It freshes the upper surface and coin the salinity difference (Figure). Since salinity for such cold ocean temperature (Figure) defines the state of the ocean and, therefore, determines the ocean's dynamical behavior, this salinity bias has consequences for the coupling of EC-Earth with PISM.

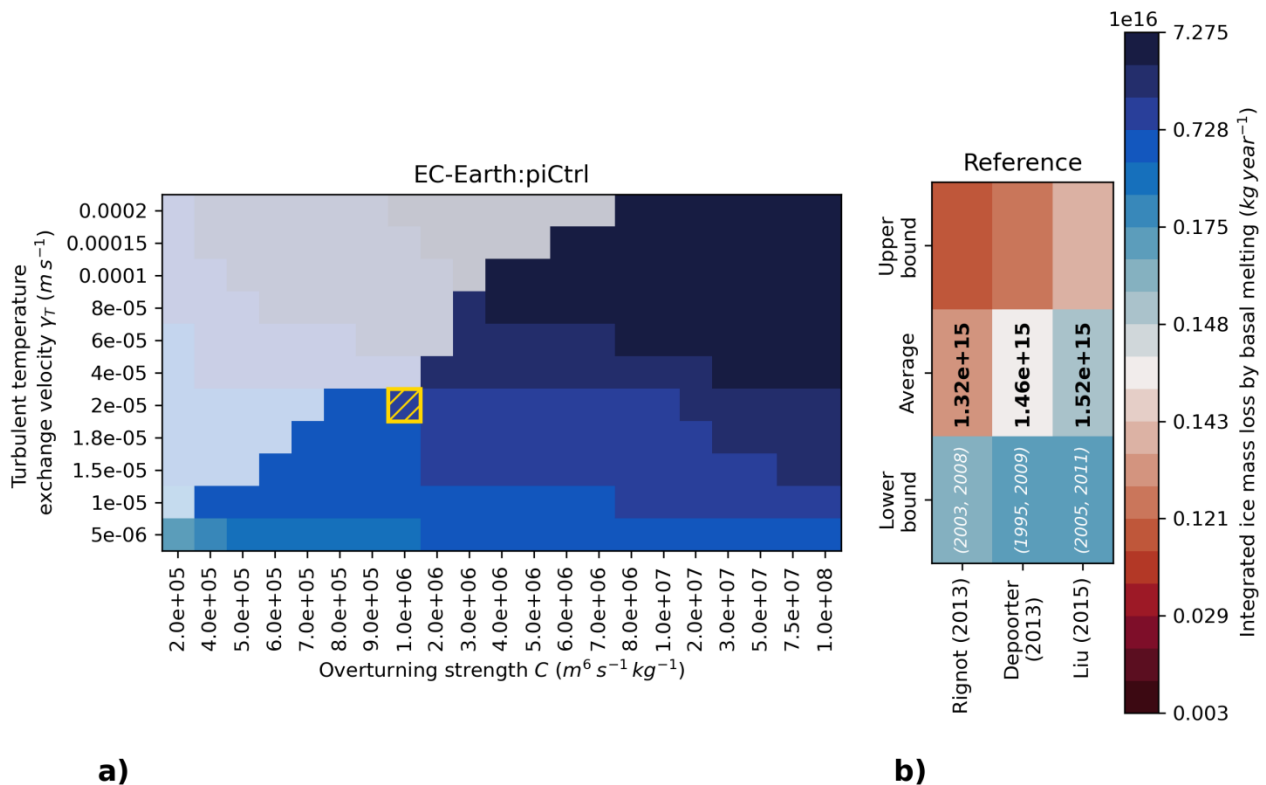


**Figure 13** The left subplot a) shows integrated ice mass loss by basal melting for an ice sheet geometry retrieved from BEDMAP2 (Fretwell et al., 2013). Here we use the ocean data coming directly from the EC-Earth model. We vary along the x-axis the Overturning strength, and along the y-axis the turbulent exchange velocity for temperature. The right subplot b) shows estimates of the basal melting, including the uncertainties. Blue colors stand for an integrated melting rate exceeding the average mean observational estimate, while a red color illustrates an underestimation. Those parts in subplot a) with faded colors do not fulfill the additional constraints. Hence, the related combinations are invalid. The yellow box in the subplot a) highlights the reference value found in the PICO publication (Reese et al., 2018a).

The too warm ocean in front of the West Antarctic Ice Sheet prevents a direct coupling because the thermal driving would trigger a widespread disintegration of the West Antarctic Ice Sheet, as preliminary standalone ice sheet simulations suggest (not shown).

Furthermore, the search for reasonable parameters controlling the PICO submodel highlights that the direct application of EC-Earth's climate fields may hinder us from representing the Antarctic ice sheet in a coupled system realistically. Therefore, we decide to use an anomaly coupling approach. Currently, we apply the EC-Earth atmospheric anomaly forcing field on the top of the RACMO estimates. We consider replacing RACMO with HIRHAM depending on the coming progress. In addition, we add oceanographic anomaly fields from EC-Earth on top of ISMIP6. Again, we prepare for replacing ISMIP6 with WOA18 because we have found substantial differences in some basins.

## 8.2 Examples of transformed fields from EC-Earth to PISM and vice versa

The workflow of the coupling is described in the publication of Gierz et al. (Gierz et al., 2020). To get an impression of the step, we examine one exchange of fields from the atmosphere model IFS to the ice sheet model PISM and vice versa (Figure). Afterward, we show an example for the transfer between the ocean model NEMO and PISM (Figure).

To drive the PDD to determine the surface mass balance, PISM requires the total precipitation and the 2m-air temperature. The latter is also used to determine the temperature of the ice surface. Therefore, 6-hourly IFS output data files in the GRIB format are transformed to the PISM grid (Figure a, b). After the PISM run,

the updated ice sheet topography expressed as surface elevation is converted back onto the IFS grid ( Figurec, d). The updated surface elevation on the IFS grid contains only the part covered by the PISM domain. Therefore an additional step, which merges the topography beyond the PISM domain, is required before IFS gets an updated global orography.

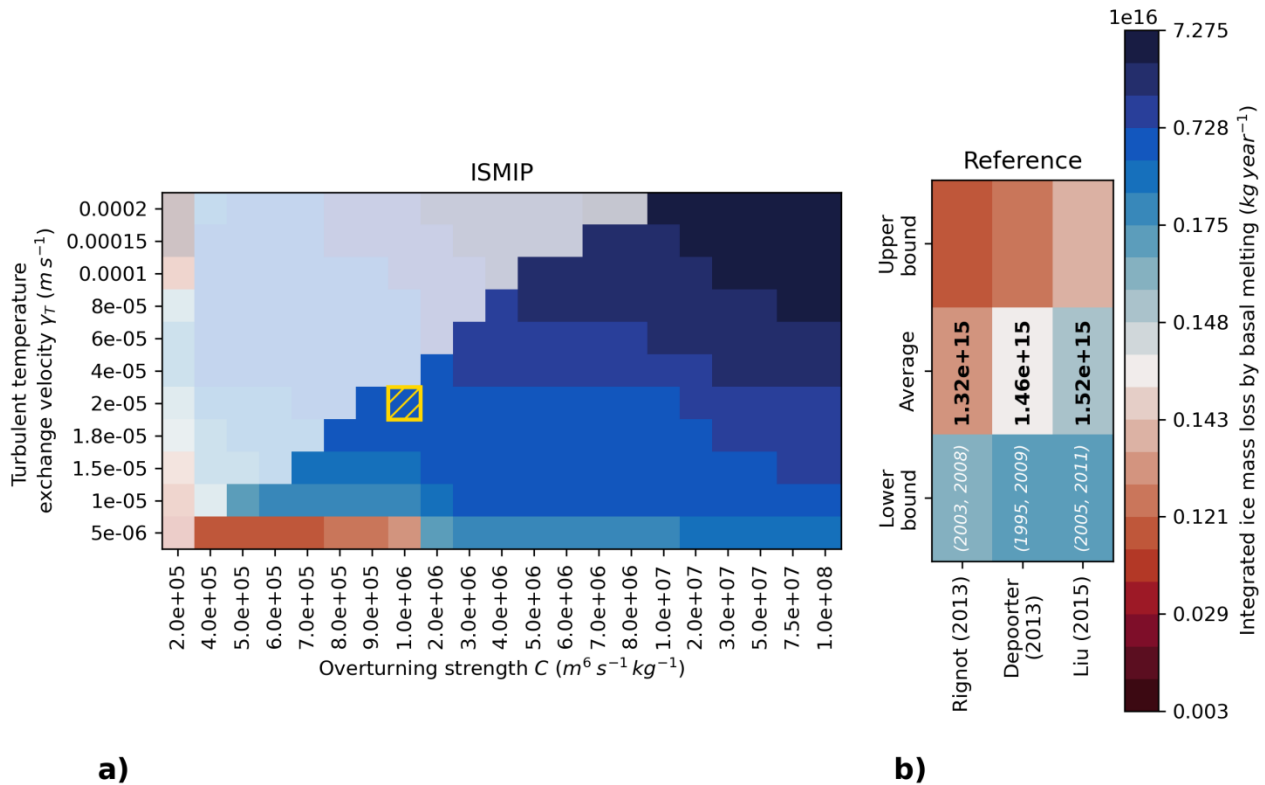


**Figure 14** Like Figure 13, but we use the ISMIP6 data set (Jourdain et al., 2020) to force PICO (Reese et al., 2018a).

The same workflow is used for the exchange between the ocean model NEMO and PISM. Since the ice shelf parameterization PICO needs a two-dimensional field in the XY-plane, we average the ocean temperature in the vertical. The average is computed between 200 m and 700 m because the inflow of water into the ice shelves occurs near the ocean floor. The floor's depth is defined by glacial scraped troughs in the continental shelf and broader continental shelf, which has an average depth of about 500 m around Antarctica. The vertical average ocean temperature is regridded onto the PISM grid and extrapolated into the ice shelf caverns. For the extrapolation, a distance-weighted approach is used. Therefore, the ocean temperature between the western and eastern Ross Ice Shelf differs ( Figureb). However, the PICO model computes the basal melting for predefined basins, and the entire Ross Ice Shelf is part of one basin in our setup. A mean temperature that is characteristic for each basin is applied in PICO. This procedure smooths small scale variations as those identified in the Ross Ice Shelf.

As part of the PISM simulation, the iceberg calving and basal melting in ice shelf caverns are computed and written into a file. These fields are regridded after the PISM simulation onto the NEMO grid, as shown in Figurec, d. Since the NEMO grid does not cover the entire Ross Ice Shelf nor Filchner-Ronne Ice Shelf, the simple regridding would miss the basal melt flux at the southernmost edge. Therefore, a rescaling is necessary to close the freshwater budget. Furthermore, the freshwater input regridded on the ocean model's land point needed to be reshuffled into the ocean. Since this is working in progress, we use a temporary solution. For the time being, all freshwater is transferred onto the atmosphere grid, where the hydrological scheme routes the freshwater, as it does for precipitation, to the coastal ocean. There it is finally released into the surface ocean. This procedure has been tested in the coupled setup of PISM and AWI- CM (Gierz et al., 2020).

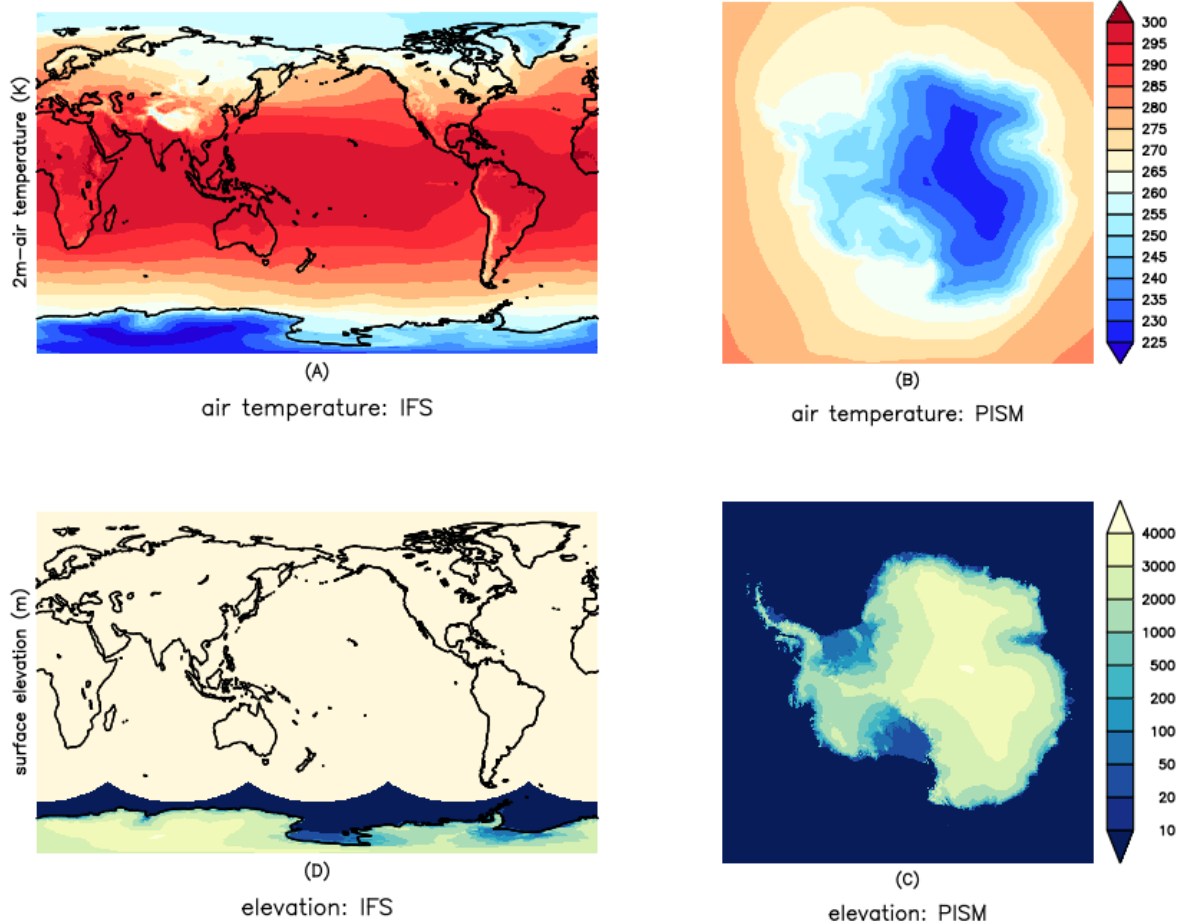


**Figure 15** Example of fields exchanged between the atmosphere model IFS and the ice sheet model PISM. The annual 2m-air temperature distribution on the native IFS grid (A, upper left) is transformed via SCOPE to the native PISM grid (B, upper right) to drive the PISM simulations. After the PISM run, an updated surface elevation of the ice sheet (C, lower right) is transformed on the IFS grid (D, lower left).

## 9 Conclusion

A preliminary setup that couples the climate model EC-Earth and the ice sheet model PISM representing the Antarctic Ice Sheet has been developed. The first results are encouraging and highlight that the applied coupling strategy seems to work. However, we need to finalize PISM's initial state before long-term coupled simulations can be performed. Also, we haven't decided about the final reference which will be used for the anomaly coupling. For the atmosphere side, we will either use RACMO or HIRHAM. We will choose between the World Ocean Atlas 2018 or the ISMIP6 data set (Jourdain et al., 2020) as oceanographic reference. In the longer-term, we plan to adapt a more sophisticated surface mass balance model. It will represent already seen changes as the two-week-long melting event in West Antarctica in 2016 (Nicolas et al., 2017). We will do these tasks in collaboration with the work dedicated to integrating the Greenland Ice Sheet. We envision a system that contains both ice sheets, Greenland and Antarctic, to disentangle reciprocal links that may amplify or damp a changing global climate system.

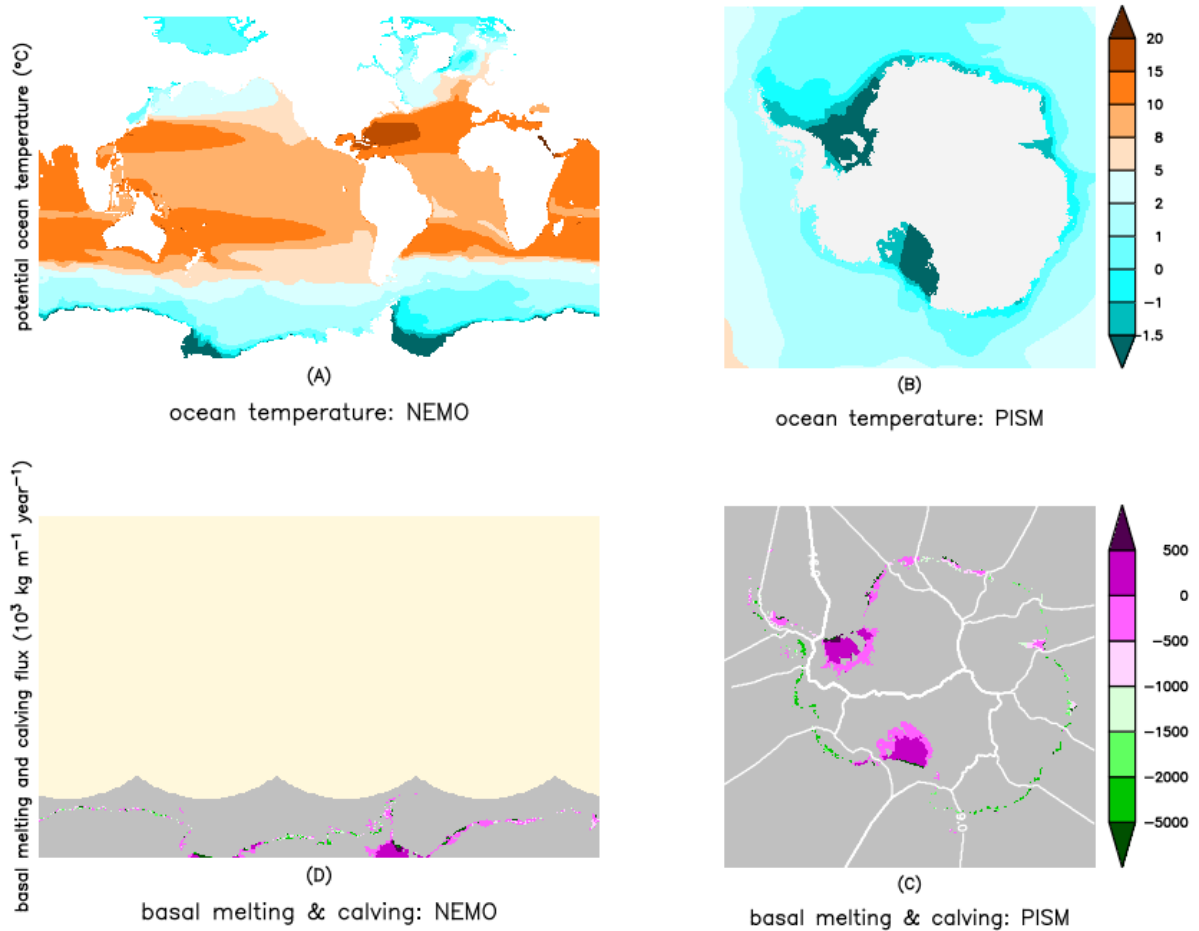


**Figure 16** Example of fields exchanged between the ocean model NEMO and the ice sheet model PISM. The annual potential ocean temperature distribution on the native NEMO grid (A, upper left) is transformed via SCOPE to the native PISM grid (B, upper right) to drive the PISM simulations. After the PISM run, basal melting and calving fluxes of the ice sheet (C, lower right) is transformed onto the NEMO grid (D, lower left). The white lines in the lower right subfigure (C) follows the defined basins used by the PICO model.

## 10 Appendix

In SCOPE, the transformation of fields between different model grids is controlled by a YAML-configuration file. The file used to produce the files shown in the Figure and Figure follows below.

```
#
# Usage: scope send|receive YAML-file ifs|nemo|pism
#
template_replacements:
  EXP_ID: "p001"
  LEG_NUMBER: "002"
  COUPLE_SUBDIR: "pism.couple"
  DATA_DIR: "/work/diskspace/UserName/ecearth3_exp/"
  ROOT_DIR: "/work/diskspace/UserName/ecearth3_exp/"
  COUPLE_SUBDIR: "pism.couple"
  DATE_PATTERN_6: "[0-9]{6}"
  DATE_PATTERN_8: "[0-9]{8}"

# -----
scope:
  couple_dir: "{{ ROOT_DIR }}/{{ EXP_ID }}/{{ COUPLE_SUBDIR }}"
  "number openMP processes": 8

# -----
#
# IFS atmosphere
#
ifs:
  type: atmosphere
  griddes: T255grid
  outdata_dir: "{{ DATA_DIR }}/{{ EXP_ID }}/output/ifs/{{ LEG_NUMBER }}"
  code_table: "ecmwf"
  pre_send:
    program: "echo '*** IFS is ready to send: >>{{ COUPLE_SUBDIR }}<< ***'"
  post_send:
    program: "cdo -O -t ecmwf -f nc setgridtype,regular -monmean -shifttime,-
1sec {{ ROOT_DIR }}/{{ EXP_ID }}/{{ COUPLE_SUBDIR }}/atmosphere_file_for_ice.dat
atm.tmp; mv atm.tmp {{ ROOT_DIR }}/{{ EXP_ID }}/{{ COUPLE_SUBDIR
}}/atmosphere_file_for_ice.dat; echo '*** IFS completed sending ***'"
  send:
    ice:
      T2M:
        files:
          pattern: "ICMGG{{ EXP_ID }}\\+{{ DATE_PATTERN_6 }}"
          take:
            what: files
            newest: "{{ 4 * 365 }}"
        cdo:
          - "-setgrid,T255"
          - "-shifttime,-1sec"
          - "-monmean"
        code_table: "ecmwf"
        convert_to_netcdf: False
  recieve:
```

```

ice:
  usurf:
    interp: bil
    target_file: "{{ ROOT_DIR }}/{{ EXP_ID }}/{{ COUPLE_SUBDIR
    }}/ice2atm_given_file.nc"
    cdo:
      - "expr,'elevation=usurf'"
      - "setunit,'m'"
      # - "expr,'geosp=usurf*9.81'"
      # - "setunit,'m-2 s-2'"
# -----
#
# NEMO Ocean
#
nemo:
  type: ocean
  griddes: "/home/UserName/share/SCOPE/ECE2PISM/ocean.ORCA1L75.griddes"
  outdata_dir: "{{ ROOT_DIR }}/{{ EXP_ID }}/output/nemo/{{ LEG_NUMBER }}"
  pre_send:
    program: "echo '*** NEMO is ready to send: >>{{ COUPLE_SUBDIR }}<< ***'"
  post_send:
    program: "cdo -timmean {{ ROOT_DIR }}/{{ EXP_ID }}/{{ COUPLE_SUBDIR
    }}/ocean_file_for_ice.dat oce.tmp; mv oce.tmp {{ ROOT_DIR }}/{{ EXP_ID }}/{{
    COUPLE_SUBDIR }}/ocean_file_for_ice.dat; echo '*** NEMO completed sending ***'"

  send:
    ice:
      thetao:
        files:
          pattern: "{{ EXP_ID }}_1m_{{ DATE_PATTERN_8 }}_{{ DATE_PATTERN_8
          }}_grid_T.nc"
        take:
          what: files
          newest: 1
  recieve:
    ice:
      ice2oce_flux:
        interp: bil
        receive_from: [basal_mass_flux_floating,
        tendency_of_ice_amount_due_to_discharge]
        target_file: "{{ ROOT_DIR }}/{{ EXP_ID }}/{{ COUPLE_SUBDIR
        }}/ice2atm_given_file.nc"
        cdo:
          - expr,'ice2oce_flux
          =(basal_mass_flux_floating+tendency_of_ice_amount_due_to_discharge)'"
# -----
#
# PISM ice sheet
#
pism:
  type: ice
  griddes: "/home/UserName/share/SCOPE/ECE2PISM/Antarctica/ice.griddes"

```

```

outdata_dir: "{{ ROOT_DIR }}/{{ EXP_ID }}/PISM/PISM_{{ EXP_ID }}/save/extra"
pre_send:
  program: "echo '*** PISM is ready to send: >>{{ COUPLE_SUBDIR }}<< ***'"
post_send:
  program: "echo '*** PISM completed sending ***'"
recieve:
  atmosphere:
    T2M:
      interp: bil
      target_file: "{{ ROOT_DIR }}/{{ EXP_ID }}/{{ COUPLE_SUBDIR
}}/atmosphere_given_file.nc"
      cdo:
        - "timmean"
        - "setreftime,0000-01-01,00:00:00"
        - "settaxis,0000-01-01,00:00:00"
        - "setunit,Kelvin"
        - "expr,'air_temp=T2M'"
    ocean:
      theta:
        interp: bil
        target_file: "{{ ROOT_DIR }}/{{ EXP_ID }}/{{ COUPLE_SUBDIR
}}/ocean_given_file.nc"
        cdo:
          - "timmean"
          - "setreftime,0000-01-01,00:00:00"
          - "settaxis,0000-01-01,00:00:00"
          - "setunit,Kelvin"
          - "expr,theta_ocean=theta+273.15"
          - "sellevidx,31/42"
          - setmisstodis
          - vertmean
send:
  atmosphere:
    usurf:
      files:
        pattern: "PISM_{{ EXP_ID }}.extra.*.nc"
        take:
          what: files
          newest: 1
    ocean:
      basal_mass_flux_floating:
        files:
          pattern: "PISM_{{ EXP_ID }}.extra.*.nc"
          take:
            what: files
            newest: 1
      tendency_of_ice_amount_due_to_discharge:
        files:
          pattern: "PISM_{{ EXP_ID }}.extra.*.nc"
          take:
            what: files
            newest: 1
#

```

# -----  
# -- last line

## 11 References

- Abe-Ouchi, A., Saito, F., Kawamura, K., Raymo, M. E., Okuno, J., Takahashi, K. and Blatter, H.: Insolation-driven 100,000-year glacial cycles and hysteresis of ice-sheet volume, *Nature*, 500(7461), 190–193, doi:10.1038/nature12374, 2013.
- Agosta, C., Amory, C., Kittel, C., Orsi, A., Favier, V., Gallée, H., van den Broeke, M. R., Lenaerts, J. T. M., van Wessem, J. M., van de Berg, W. J. and Fettweis, X.: Estimation of the Antarctic surface mass balance using the regional climate model MAR (1979–2015) and identification of dominant processes, *Cryosph.*, 13(1), 281–296, doi:10.5194/tc-13-281-2019, 2019.
- Asay-Davis, X. S.: Final Report: Modeling coupled ice sheet-ocean interactions in the Model for Prediction Across Scales (MPAS) and in DOE Earth System Models, , 13p, doi:10.2172/1490084, 2019.
- Bell, R. E., Banwell, A. F., Trusel, L. D. and Kingslake, J.: Antarctic surface hydrology and impacts on ice-sheet mass balance, *Nat. Clim. Chang.*, 8(12), 1044–1052, doi:10.1038/s41558-018-0326-3, 2018.
- Bromwich, D. H., Nicolas, J. P. and Monaghan, A. J.: An Assessment of Precipitation Changes over Antarctica and the Southern Ocean since 1989 in Contemporary Global Reanalyses, *J. Clim.*, 24(16), 4189–4209, doi:10.1175/2011JCLI4074.1, 2011.
- Bueler, E. and Brown, J.: Shallow shelf approximation as a “sliding law” in a thermomechanically coupled ice sheet model, *J. Geophys. Res.*, 114(F3), F03008, doi:10.1029/2008JF001179, 2009.
- Bueler, E., Lingle, C. S. and Brown, J.: Fast computation of a viscoelastic deformable Earth model for ice-sheet simulations, *Ann. Glaciol.*, 46, 97–105, doi:10.3189/172756407782871567, 2007.
- Clem, K. R., Fogt, R. L., Turner, J., Lintner, B. R., Marshall, G. J., Miller, J. R. and Renwick, J. A.: Record warming at the South Pole during the past three decades, *Nat. Clim. Chang.*, 10(8), 762–770, doi:10.1038/s41558-020-0815-z, 2020.
- Craig, A., Valcke, S. and Coquart, L.: Development and performance of a new version of the OASIS coupler, OASIS3-MCT\_3.0, *Geosci. Model Dev.*, 10(9), 3297–3308, doi:10.5194/gmd-10-3297-2017, 2017.
- Cunningham, S. A.: Transport and variability of the Antarctic Circumpolar Current in Drake Passage, *J. Geophys. Res.*, 108(C5), 1–17, doi:10.1029/2001jc001147, 2003.
- Darelius, E., Fer, I. and Nicholls, K. W.: Observed vulnerability of Filchner-Ronne Ice Shelf to wind-driven inflow of warm deep water, *Nat. Commun.*, 7(1), 12300, doi:10.1038/ncomms12300, 2016.
- Depoorter, M. , Bamber, J. L., Griggs, J. A., Lenaerts, J. T. M., Ligtenberg, S. R. M., van den Broeke, M. R. and Moholdt, G.: Calving fluxes and basal melt rates of Antarctic ice shelves., *Nature*, 502(7469), 89–92, doi:10.1038/nature12567, 2013.

Dinniman, M., Asay-Davis, X., Galton-Fenzi, B., Holland, P., Jenkins, A. and Timmermann, R.: Modeling Ice Shelf/Ocean Interaction in Antarctica: A Review, *Oceanography*, 29(4), 144–153, doi:10.5670/oceanog.2016.106, 2016.

Donohue, K. A., Tracey, K. L., Watts, D. R., Chidichimo, M. P. and Chereskin, T. K.: Mean Antarctic Circumpolar Current transport measured in Drake Passage, *Geophys. Res. Lett.*, 43(22), 11760–11767, doi:10.1002/2016GL070319, 2016.

Favier, L., Jourdain, N. C., Jenkins, A., Merino, N., Durand, G., Gagliardini, O., Gillet-Chaulet, F. and Mathiot, P.: Assessment of sub-shelf melting parameterisations using the ocean–ice-sheet coupled model NEMO(v3.6)–Elmer/Ice(v8.3), *Geosci. Model Dev.*, 12(6), 2255–2283, doi:10.5194/gmd-12-2255-2019, 2019.

Feldmann, J., Albrecht, T., Khroulev, C., Pattyn, F. and Levermann, A.: Resolution-dependent performance of grounding line motion in a shallow model compared with a full-Stokes model according to the MISIMP3d intercomparison, *J. Glaciol.*, 60(220), 353–360, doi:10.3189/2014JoG13J093, 2014.

Fretwell, P., Pritchard, H. D., Vaughan, D. G., Bamber, J. L., Barrand, N. E., Bell, R., Bianchi, C., Bingham, R. G., Blankenship, D. D., Casassa, G., Catania, G., Callens, D., Conway, H., Cook, A. J., Corr, H. F. J., Damaske, D., Damm, V., Ferraccioli, F., Forsberg, R., Fujita, S., Gim, Y., Gogineni, P., Griggs, J. A., Hindmarsh, R. C. A., Holmlund, P., Holt, J. W., Jacobel, R. W., Jenkins, A., Jokat, W., Jordan, T., King, E. C., Kohler, J., Krabill, W., Riger-Kusk, M., Langley, K. A., Leitchenkov, G., Leuschen, C., Luyendyk, B. P., Matsuoka, K., Mouginot, J., Nitsche, F. O., Nogi, Y., Nost, O. A., Popov, S. V., Rignot, E., Ripplin, D. M., Rivera, A., Roberts, J., Ross, N., Siegert, M. J., Smith, A. M., Steinhage, D., Studinger, M., Sun, B., Tinto, B. K., Welch, B. C., Wilson, D., Young, D. A., Xiangbin, C. and Zirizzotti, A.: Bedmap2: improved ice bed, surface and thickness datasets for Antarctica, *Cryosph.*, 7(1), 375–393, doi:10.5194/tc-7-375-2013, 2013.

Frieler, K., Clark, P. U., He, F., Buizert, C., Reese, R., Ligtenberg, S. R. M., van den Broeke, M. R., Winkelmann, R. and Levermann, A.: Consistent evidence of increasing Antarctic accumulation with warming, *Nat. Clim. Chang.*, 5(4), 348–352, doi:10.1038/nclimate2574, 2015.

Garbe, J., Albrecht, T., Levermann, A., Donges, J. F. and Winkelmann, R.: The hysteresis of the Antarctic Ice Sheet, *Nature*, 585(7826), 538–544, doi:10.1038/s41586-020-2727-5, 2020.

Gierz, P., Ackermann, L., Rodehacke, C., Krebs-Kanzow, U., Stepanek, C., Barbi, D. and Lohmann, G.: Simulating interactive ice sheets in the multi-resolution AWI-ESM 1.2: A case study using SCOPE 1.0, *Geosci. Model Dev. Discuss.*, 1–32, doi:10.5194/gmd-2020-159, 2020.

Goldberg, D. N., Gourmelen, N., Kimura, S., Millan, R. and Snow, K.: How Accurately Should We Model Ice Shelf Melt Rates?, *Geophys. Res. Lett.*, 46(1), 189–199, doi:10.1029/2018GL080383, 2019.

Golledge, N. R., Kowalewski, D. E., Naish, T. R., Levy, R. H., Fogwill, C. J. and Gasson, E. G. W.: The multi-millennial Antarctic commitment to future sea-level rise, *Nature*, 526(7573), 421–425, doi:10.1038/nature15706, 2015.

Golledge, N. R., Keller, E. D., Gomez, N., Naughten, K. A., Bernales, J., Trusel, L. D. and Edwards, T. L.: Global environmental consequences of twenty-first-century ice-sheet melt, *Nature*, 566(7742), 65–72, doi:10.1038/s41586-019-0889-9, 2019.

Gürses, Ö., Kolatschek, V., Wang, Q. and Rodehacke, C. B.: Brief communication: A submarine wall protecting the Amundsen Sea intensifies melting of neighboring ice shelves, *Cryosph.*, 13(9), 2317–2324, doi:10.5194/tc-13-2317-2019, 2019.

Harig, C. and Simons, F. J.: Accelerated West Antarctic ice mass loss continues to outpace East Antarctic gains, *Earth Planet. Sci. Lett.*, 415, 134–141, doi:10.1016/j.epsl.2015.01.029, 2015.

Hock, R.: Temperature index melt modelling in mountain areas, *J. Hydrol.*, 282(1–4), 104–115, doi:10.1016/S0022-1694(03)00257-9, 2003.

Jenkins, A., Shoosmith, D., Dutrieux, P., Jacobs, S., Kim, T. W., Lee, S. H., Ha, H. K. and Stammerjohn, S.: West Antarctic Ice Sheet retreat in the Amundsen Sea driven by decadal oceanic variability, *Nat. Geosci.*, 11(10), 733–738, doi:10.1038/s41561-018-0207-4, 2018.

Jourdain, N. C., Asay-Davis, X., Hattermann, T., Straneo, F., Seroussi, H., Little, C. M. and Nowicki, S.: A protocol for calculating basal melt rates in the ISMIP6 Antarctic ice sheet projections, *Cryosph.*, 14(9), 3111–3134, doi:10.5194/tc-14-3111-2020, 2020.

Kayastha, R. B., Takeuchi, Y., Nakawo, M. and Ageta, Y.: Practical prediction of ice melting beneath various thickness of debris cover on Khumbu Glacier, Nepal, using a positive degree-day factor, in *IAHS Publication*, pp. 71–81, IAHS Press - Intern. Assoc. Hydrological Science, Seattle, Washington, USA., 2000.

Khazendar, A., Rignot, E., Schroeder, D. M., Seroussi, H., Schodlok, M. P., Scheuchl, B., Mouginot, J., Sutterley, T. C. and Velicogna, I.: Rapid submarine ice melting in the grounding zones of ice shelves in West Antarctica, *Nat. Commun.*, 7, 13243, doi:10.1038/ncomms13243, 2016.

Kreuzer, M., Reese, R., Huiskamp, W. N., Petri, S., Albrecht, T., Feulner, G. and Winkelmann, R.: Coupling framework (1.0) for the ice sheet model PISM (1.1.1) and the ocean model MOM5 (5.1.0) via the ice-shelf cavity module PICO, *Geosci. Model Dev. Discuss.*, 1–21, doi:10.5194/gmd-2020-230, 2020.

Krinner, G., Magand, O., Simmonds, I., Genthon, C. and Dufresne, J.-L.: Simulated Antarctic precipitation and surface mass balance at the end of the twentieth and twenty-first centuries, *Clim. Dyn.*, 28(2–3), 215–230, doi:10.1007/s00382-006-0177-x, 2006.

Kuipers Munneke, P., Picard, G., van den Broeke, M. R., Lenaerts, J. T. M. and van Meijgaard, E.: Insignificant change in Antarctic snowmelt volume since 1979, *Geophys. Res. Lett.*, 39(L01501), 5pp, doi:10.1029/2011GL050207, 2012.

Kuipers Munneke, P., Luckman, A. J., Bevan, S. L., Smeets, C. J. P. P., Gilbert, E., van den Broeke, M. R., Wang, W., Zender, C., Hubbard, B., Ashmore, D., Orr, A., King, J. C. and Kulesa, B.: Intense Winter Surface Melt on an Antarctic Ice Shelf, *Geophys. Res. Lett.*, 45(15), 7615–7623, doi:10.1029/2018GL077899, 2018.

Langen, P. L., Mottram, R. H., Christensen, J. H., Boberg, F., Rodehacke, C. B., Stendel, M., van As, D., Ahlstrøm, A. P., Mortensen, J., Rysgaard, S., Petersen, D., Svendsen, K. H., Aðalgeirsdóttir, G. and Cappelen, J.: Quantifying energy and mass fluxes controlling Godthåbsfjord freshwater input in a 5 km simulation (1991–2012), *J. Clim.*, 28(9), 3694–3713, doi:10.1175/JCLI-D-14-00271.1, 2015.

Levermann, A., Albrecht, T., Winkelmann, R., Martin, M. A., Haseloff, M. and Joughin, I.: Kinematic first-order calving law implies potential for abrupt ice-shelf retreat, *Cryosph.*, 6(2), 273–286, doi:10.5194/tc-6-273-2012, 2012.

Lingle, C. S. and Clark, J. A.: A numerical model of interactions between a marine ice sheet and the solid earth: Application to a West Antarctic ice stream, *J. Geophys. Res.*, 90(C1), 1100–1114, doi:10.1029/JC090iC01p01100, 1985.

- Liston, G. E. and Winther, J.-G.: Antarctic Surface and Subsurface Snow and Ice Melt Fluxes, *J. Clim.*, 18(10), 1469–1481, doi:10.1175/JCLI3344.1, 2005.
- Liu, Y., Moore, J. C., Cheng, X., Gladstone, R. M., Bassis, J. N., Liu, H., Wen, J. and Hui, F.: Ocean-driven thinning enhances iceberg calving and retreat of Antarctic ice shelves, *Proc. Natl. Acad. Sci.*, 112(11), 3263–3268, doi:10.1073/pnas.1415137112, 2015.
- Lythe, M. B. and Vaughan, D. G.: BEDMAP: A new ice thickness and subglacial topographic model of Antarctica, *J. Geophys. Res. Solid Earth*, 106(B6), 11335–11351, doi:10.1029/2000JB900449, 2001.
- Medley, B. and Thomas, E. R.: Increased snowfall over the Antarctic Ice Sheet mitigated twentieth-century sea-level rise, *Nat. Clim. Chang.*, 9(1), 34–39, doi:10.1038/s41558-018-0356-x, 2019.
- Mengel, M., Feldmann, J. and Levermann, A.: Linear sea-level response to abrupt ocean warming of major West Antarctic ice basin, *Nat. Clim. Chang.*, 6(1), 71–74, doi:10.1038/nclimate2808, 2015.
- Mercer, J. H.: West Antarctic ice sheet and CO<sub>2</sub> greenhouse effect: a threat of disaster, *Nature*, 271(5643), 321–325, doi:10.1038/271321a0, 1978.
- Milillo, P., Rignot, E., Rizzoli, P., Scheuchl, B., Mouginot, J., Bueso-Bello, J. and Prats-Iraola, P.: Heterogeneous retreat and ice melt of Thwaites Glacier, West Antarctica, *Sci. Adv.*, 5(1), eaau3433, 8pp, doi:10.1126/sciadv.aau3433, 2019.
- Moore, J. C., Gladstone, R., Zwinger, T. and Wolovick, M.: Geoengineer polar glaciers to slow sea-level rise, *Nature*, 555(7696), 303–305, doi:10.1038/d41586-018-03036-4, 2018.
- Morlighem, M., Rignot, E., Binder, T., Blankenship, D., Drews, R., Eagles, G., Eisen, O., Ferraccioli, F., Forsberg, R., Fretwell, P., Goel, V., Greenbaum, J. S., Gudmundsson, H., Guo, J., Helm, V., Hofstede, C., Howat, I., Humbert, A., Jokati, W., Karlsson, N. B., Lee, W. S., Matsuoka, K., Millan, R., Mouginot, J., Paden, J., Pattyn, F., Roberts, J., Rosier, S., Ruppel, A., Seroussi, H., Smith, E. C., Steinhage, D., Sun, B., Broeke, M. R. van den, Ommen, T. D. van, Wessem, M. van and Young, D. A.: Deep glacial troughs and stabilizing ridges unveiled beneath the margins of the Antarctic ice sheet, *Nat. Geosci.*, 13(2), 132–137, doi:10.1038/s41561-019-0510-8, 2020.
- Mottram, R., Boberg, F., Langen, P., Yang, S., Rodehacke, C., Christensen, J. H. and Madsen, M. S.: Surface mass balance of the Greenland ice sheet in the regional climate model HIRHAM5: Present state and future prospects, *Low Temp. Sci.*, 75, 105–115, doi:10.14943/lowtempsci.75.105, 2017.
- Nakayama, Y., Timmermann, R., Schröder, M. and Hellmer, H. H.: On the difficulty of modeling Circumpolar Deep Water intrusions onto the Amundsen Sea continental shelf, *Ocean Model.*, 84, 26–34, doi:10.1016/j.ocemod.2014.09.007, 2014.
- Nicolas, J. P., Vogelmann, A. M., Scott, R. C., Wilson, A. B., Cadeddu, M. P., Bromwich, D. H., Verlinde, J., Lubin, D., Russell, L. M., Jenkinson, C., Powers, H. H., Ryczek, M., Stone, G. and Wille, J. D.: January 2016 extensive summer melt in West Antarctica favoured by strong El Niño, *Nat. Commun.*, 8(15799), 10p, doi:10.1038/ncomms15799, 2017.
- Olbers, D. and Hellmer, H.: A box model of circulation and melting in ice shelf caverns, *Ocean Dyn.*, 60(1), 141–153, doi:10.1007/s10236-009-0252-z, 2010.

Pattyn, F.: The paradigm shift in Antarctic ice sheet modelling, *Nat. Commun.*, 9(1), 2728, doi:10.1038/s41467-018-05003-z, 2018.

Reeh, N.: Parameterization of melt rate and surface temperature on the Greenland Ice Sheet, *Polarforschung*, 59(3), 113–128 [online] Available from: <http://hdl.handle.net/10013/epic.29636>, 1991.

Reese, R., Albrecht, T., Mengel, M., Asay-Davis, X. and Winkelmann, R.: Antarctic sub-shelf melt rates via PICO, *Cryosph.*, 12(6), 1969–1985, doi:10.5194/tc-12-1969-2018, 2018.

Rignot, E., Jacobs, S., Mouginot, J. and Scheuchl, B.: Ice-Shelf Melting Around Antarctica, *Science* (80-. ), 341(6143), 266–270, doi:10.1126/science.1235798, 2013.

Rignot, E., Mouginot, J., Morlighem, M., Seroussi, H. and Scheuchl, B.: Widespread, rapid grounding line retreat of Pine Island, Thwaites, Smith, and Kohler glaciers, West Antarctica, from 1992 to 2011, *Geophys. Res. Lett.*, 41(10), 3502–3509, doi:10.1002/2014GL060140, 2014.

Rignot, E., Mouginot, J., Scheuchl, B., van den Broeke, M., van Wessem, M. J. and Morlighem, M.: Four decades of Antarctic Ice Sheet mass balance from 1979–2017, *Proc. Natl. Acad. Sci.*, 116(4), 1095–1103, doi:10.1073/pnas.1812883116, 2019.

Rignot, E., Box, J. E., Burgess, E. and Hanna, E.: Mass balance of the Greenland Ice Sheet from 1992 to 2018, *Nature*, 579(7798), 233–239, doi:10.1038/s41586-019-1855-2, 2020.

Rodehacke, C. B., Pfeiffer, M., Semmler, T., Gurses, Ö. and Kleiner, T.: Future sea level contribution from Antarctica inferred from CMIP5 model forcing and its dependence on precipitation ansatz, *Earth Syst. Dyn.*, 11(4), 1153–1194, doi:10.5194/esd-11-1153-2020, 2020.

Sadai, S., Condron, A., DeConto, R. and Pollard, D.: Future climate response to Antarctic Ice Sheet melt caused by anthropogenic warming, *Sci. Adv.*, 6(39), eaaz1169, 8pp, doi:10.1126/sciadv.aaz1169, 2020.

Sasgen, I., van den Broeke, M., Bamber, J. L., Rignot, E., Sørensen, L. S., Wouters, B., Martinec, Z., Velicogna, I. and Simonsen, S. B.: Timing and origin of recent regional ice-mass loss in Greenland, *Earth Planet. Sci. Lett.*, 333–334, 293–303, doi:10.1016/j.epsl.2012.03.033, 2012.

Schlatter, T. W.: The Local Surface Energy Balance and Subsurface Temperature Regime in Antarctica, *J. Appl. Meteorol.*, 11(7), 1048–1062, doi:10.1175/1520-0450(1972)011<1048:TLSEBA>2.0.CO;2, 1972.

Schoof, C.: A variational approach to ice stream flow, *J. Fluid Mech.*, 556, 227–251, doi:10.1017/S0022112006009591, 2006.

Shepherd, A., Ivins, E. R., Geruo, A., Barletta, V. R., Bentley, M. J., Bettadpur, S., Briggs, K. H., Bromwich, D. H., Forsberg, R., Galin, N., Horwath, M., Jacobs, S., Joughin, I., King, M. A., Lenaerts, J. T. M., Li, J., Ligtenberg, S. R. M., Luckman, A., Luthcke, S. B., McMillan, M., Meister, R., Milne, G., Mouginot, J., Muir, A., Nicolas, J. P., Paden, J., Payne, A. J., Pritchard, H., Rignot, E., Rott, H., Sorensen, L. S., Scambos, T. A., Scheuchl, B., Schrama, E. J. O., Smith, B., Sundal, A. V., van Angelen, J. H., van de Berg, W. J., van den Broeke, M. R., Vaughan, D. G., Velicogna, I., Wahr, J., Whitehouse, P. L., Wingham, D. J., Yi, D., Young, D. and Zwally, H. J.: A Reconciled Estimate of Ice-Sheet Mass Balance, *Science* (80-. ), 338(6111), 1183–1189, doi:10.1126/science.1228102, 2012.

Shepherd, A., Gilbert, L., Muir, A. S., Konrad, H., McMillan, M., Slater, T., Briggs, K. H., Sundal, A. V., Hogg, A. E. and Engdahl, M. E.: Trends in Antarctic Ice Sheet Elevation and Mass, *Geophys. Res. Lett.*, 46(14), 8174–8183, doi:10.1029/2019GL082182, 2019.

Siahaan, A. and Smith, R.: Preliminary results from some fully interactive UKESM1-Antarctic coupling configuration, United Kingdom. [online] Available from: <https://ukesm.ac.uk/portfolio-item/preliminary-results-ukesm1-antarctic-coupling/#>, 2019.

Smith, B., Fricker, H. A., Gardner, A. S., Medley, B., Nilsson, J., Paolo, F. S., Holschuh, N., Adusumilli, S., Brunt, K., Csatho, B., Harbeck, K., Markus, T., Neumann, T., Siegfried, M. R. and Zwally, H. J.: Pervasive ice sheet mass loss reflects competing ocean and atmosphere processes, *Science* (80-. ), 5845(February 2019), eaaz5845, 10p, doi:10.1126/science.aaz5845, 2020.

Spence, P., Griffies, S. M., England, M. H., Hogg, A. M., Saenko, O. A. and Jourdain, N. C.: Rapid subsurface warming and circulation changes of Antarctic coastal waters by poleward shifting winds, *Geophys. Res. Lett.*, 41(13), 4601–4610, doi:10.1002/2014GL060613, 2014.

Stokes, C. R., Sanderson, J. E., Miles, B. W. J., Jamieson, S. S. R. and Leeson, A. A.: Widespread distribution of supraglacial lakes around the margin of the East Antarctic Ice Sheet, *Sci. Rep.*, 9(1), 13823, doi:10.1038/s41598-019-50343-5, 2019.

Tedesco, M.: Assessment and development of snowmelt retrieval algorithms over Antarctica from K-band spaceborne brightness temperature (1979–2008), *Remote Sens. Environ.*, 113(5), 979–997, doi:10.1016/j.rse.2009.01.009, 2009.

Thompson, A. F., Stewart, A. L., Spence, P. and Heywood, K. J.: The Antarctic Slope Current in a Changing Climate, *Rev. Geophys.*, 56(4), 741–770, doi:10.1029/2018RG000624, 2018.

Timmermann, R. and Goeller, S.: Response to Filchner–Ronne Ice Shelf cavity warming in a coupled ocean–ice sheet model – Part 1: The ocean perspective, *Ocean Sci.*, 13(5), 765–776, doi:10.5194/os-13-765-2017, 2017.

Trusel, L. D., Frey, K. E., Das, S. B., Karnauskas, K. B., Kuipers Munneke, P., van Meijgaard, E. and van den Broeke, M. R.: Divergent trajectories of Antarctic surface melt under two twenty-first-century climate scenarios, *Nat. Geosci.*, 8(12), 927–932, doi:10.1038/ngeo2563, 2015.

Velicogna, I., Mohajerani, Y., A. G., Landerer, F., Mouginot, J., Noel, B., Rignot, E., Sutterley, T., Broeke, M., Wessm, M. and Wiese, D.: Continuity of Ice Sheet Mass Loss in Greenland and Antarctica From the GRACE and GRACE Follow-On Missions, *Geophys. Res. Lett.*, 47(8), 1–8, doi:10.1029/2020GL087291, 2020.

Vizcaino, M., Mikolajewicz, U., Ziemen, F., Rodehacke, C. B., Greve, R. and van den Broeke, M. R.: Coupled simulations of Greenland Ice Sheet and climate change up to A.D. 2300, *Geophys. Res. Lett.*, 42(10), 3927–3935, doi:10.1002/2014GL061142, 2015.

Webber, B. G. M., Heywood, K. J., Stevens, D. P., Dutrieux, P., Abrahamsen, E. P., Jenkins, A., Jacobs, S. S., Ha, H. K., Lee, S. H. and Kim, T. W.: Mechanisms driving variability in the ocean forcing of Pine Island Glacier, *Nat. Commun.*, 8, 1–8, doi:10.1038/ncomms14507, 2017.

Weertman, J.: Stability of the junction of an ice sheet and an ice shelf, *J. Glaciol.*, 13(67), 3–11 [online] Available from: <http://adsabs.harvard.edu/abs/1974JGlac..13....3W> (Accessed 1 October 2012), 1974.

Van Wessem, J. M., Reijmer, C. H., Morlighem, M., Mouginot, J., Rignot, E., Medley, B., Joughin, I., Wouters, B., Depoorter, M. A., Bamber, J. L., Lenaerts, J. T. M., Van De Berg, W. J., Van Den Broeke, M. R. and Van Meijgaard, E.: Improved representation of East Antarctic surface mass balance in a regional atmospheric climate model, *J. Glaciol.*, 60(222), 761–770, doi:10.3189/2014JoG14J051, 2014.

Wingham, D. J., Shepherd, A., Muir, A. and Marshall, G. J.: Mass balance of the Antarctic Ice Sheet from 1992 to 2017, *Nature*, 558(7709), 219–222, doi:10.1038/s41586-018-0179-y, 2018.

Winkelmann, R., Levermann, A., Martin, M. A. and Frieler, K.: Increased future ice discharge from Antarctica owing to higher snowfall, *Nature*, 492(7428), 239–242, doi:10.1038/nature11616, 2012.

Winkelmann, R., Levermann, A., Ridgwell, A. and Caldeira, K.: Combustion of available fossil fuel resources sufficient to eliminate the Antarctic Ice Sheet, *Sci. Adv.*, 1(8), e1500589, 5pp, doi:10.1126/sciadv.1500589, 2015.

Wolovick, M. J. and Moore, J. C.: Stopping the flood: could we use targeted geoengineering to mitigate sea level rise?, *Cryosph.*, 12(9), 2955–2967, doi:10.5194/tc-12-2955-2018, 2018.

## 12 Previous reports

Previous reports from the Danish Meteorological Institute can be found on:

<https://www.dmi.dk/publikationer/>